Discharge structure of Ar/Cl_2 inductively coupled plasma: A cyclic study of discharge conditions at fixed power

S. X. Zhao[1], A. Q. Tang[2] and Y. Tian[3]

[1] *AKey Laboratory of Material Modification by Laser, Ion, and Electron beams (Ministry of Education), School of Physics, Dalian University of Technology, 116024, Dalian, China*
[2] *China Key System & Integrated Circuit Co., Ltd, 214026, Wuxi, China*
[3] *Experimental Training Centre, Dalian University of Science and Technology, Dalian, 116052, China*

(Received: 30. March 2025, Accepted: 01. July 2025, Published online: 08. July 2025)

Discharge structure refers to the morphology of different plasma quantities, such as electron temperature, reaction rate, plasma potential, mass flux, net charge and species density, which are determined by plasma transport mechanism and chemical processes. This morphology is rather difficult to refine in complex electronegative plasma for it is contained in a multiple-physics-field coupled system. Regarding this difficulty, the combination of self-consistent simulation, theory analysis and experimental diagnostic of this system is needed. In the scope of present article, the fluid simulation and analytic theory are utilized to investigate the Ar/Cl_2 inductively coupled plasma, via a cyclic tuning of discharge pressure and feedstock gas content parameters at fixing the power. Classic discharge structure, e.g., delta, parabola, flat-top, and hollow, and specific discharge mechanisms. e.g., self-coagulation, physics coagulation, de-coagulation, grouping behaviour, and the ambi-polar diffusion of mediately electronegative plasma that is tolerant to the self-coagulation, are revealed. Besides, the two types of discharge stratification, i.e., space and species, are presented. Many non-neutralities are generated during the transport process of electronegative plasma when it gives rise to the discharge structure, which are summed and analysed for better understanding the electronegative plasmas.

(DOI: 10.31281/p8p08506)

zhaonie@dlut.edu.cn

I. Introduction

Gaseous discharge structure of laboratory plasma is very important issue, which has been investigated by many researchers. At initial, the spatially resolved plasma density, electron temperature and electric potential of argon plasma were measured by Langmuir probe [1] and validated by fluid or hybrid models [2,3]. For reactive plasmas, Han et al used the same method to investigate the electron density profile of Ar/O_2 inductively couple plasma [4]. It is noted that these comparative studies cannot reveal the transport scheme of plasma and neither explains the profile characteristics. Besides for the experiments and self-consistent simulations, early researchers still paid attention on establishing analytic theories for better understanding the discharge structure. They started from the electropositive plasma, and generated many useful conclusions by using drift-diffusion flux and continuity equation, together with the simple chemistry. Parabola, trigonometric, and Bessel distributions of plasma density were given with another approximation, ambi-polar diffusion [5]. These researchers later extended the above analytic method content and shifted it into the electronegative plasma field. They introduced the anion Boltzmann, and sequentially built the parabola (suitable for electronegative plasma), ellipse and flat-top models [6,7]. Other academicians utilized the similar analytic theory to predict the species-stratification, parabola and uniform profiles, by means of their own definitions of different models [8]. Besides, there are still many other

phenomena discovered, such as the space-stratification [9], double layer structure [10], ionic and acoustic speed at the interface of stratification [11], and general internal sheaths [12], etc. These are more about the microscopic characteristic of discharge structure. These analytic works guided well the experimental activities of that time, for many experimentalists compared their ions densities that are diagnosed in the electronegatively discharging plasma with the parabola and flat-top models [13-15].

Unfortunately, the present self-consistent simulations in the electronegative plasmas are less related to the above meaningful analytic works. Many researchers of simulation field are even not familiar with them. This leads to difficulties on analysing the simulated profiles, i.e., discharge structure. To us, not only the densities are important, but also other quantities, such as charge density, mass flux, chemical source, species velocity and so on. The present work of this article is aimed at solving this problem, taking the Ar/Cl_2 inductively coupled plasma as an example at cyclic tuning of certain discharge parameters. Together with the previous correlative works of Ar/SF_6 and Ar/O_2 inductively coupled plasmas in Refs. [16, 17] where the self-coagulation and related processes, such as scattering of the coagulated structures and blue sheath, etc., have been reported, we plan to construct the systematic discharge structure theory of electronegative plasmas, by means of first fluid model simulation, then emendation of kinetic effects, and lastly validation of experiments.

II. Fluid model and Ar/Cl_2 chemistry

As mentioned, in this work the fluid model of electronegative plasma and the analytic theory related to the discharge structure are used to analyse the Ar/Cl_2 inductive plasma mechanisms. The fluid model has been described in Ref. [16, 17], and it includes the electron equations, heavy species equations, the Maxwellian equations, and the Poisson equation, which can be solved at the certainly assigned boundary conditions, chemical reactions, surface kinetics, and reasonable transport coefficients.

After the complete physics fields are given, the fluid model is numerically solved by the finite element method. More details of the fluid model about the electronegative and inductively coupled plasma source can be found in Refs. [16, 17]. Here in this section, only the chemistry and surface kinetics as reported in Refs. [18-21] are introduced, as listed in Tabs. 1 and 2. In Ref. [22], it is reported when neglecting the charge exchange reaction between Cl^+ and Cl_2 (Reaction No. 32 in Table 1), the dependence of ion fluxes on the gas pressure and the ion energy distribution functions at the ground electrode are precisely predicted in a hybrid simulation. In the scope of present article, when the reaction No. 32 is removed, the simulated discharge structure, such as the space-stratification and double layer, is still well predicted by the fluid simulation. It is believed that the validation of numerical simulation depends on the people's deep recognitions of physical and chemical processes, not on the method of trial and error that matches the simulation to the experiment by casually adjusting the rate coefficients and surface sticking coefficients.

Regarding to the above considerations, the complete chlorine chemistry that includes the charge exchange reaction as the Refs. [19, 20, 23] did is used in this article. should be labelled as this. In Table 2, the chlorine atoms, Cl, sticking coefficient on the chamber wall surface, i.e., inorganic materials, such as metals, semiconductors and their oxides, is selected to be 0.04, as referring to the Refs. [24-26].

No.	Reaction	Rate coefficient[a]	Threshold (eV)	Ref.
1	$e + Ar \rightarrow e + Ar$	Cross Section	0	[18]
2	$e + Ar \rightarrow e + Ar^m$	Cross Section	11.6	[18]
3	$e + Ar^m \rightarrow e + Ar$	Cross Section	-11.6	[18]

4	$e + Ar \rightarrow 2e + Ar^{+}$	Cross Section	15.76	[18]
5	$e + Ar^{m} \rightarrow 2e + Ar^{+}$	Cross Section	4.43	[18]
6	$e + Cl_2 \rightarrow e + Cl_2$	Cross Section	0	[18]
7	$e + Cl \rightarrow e + Cl$	Cross Section	0	[18]
8	$e + Cl_2 \rightarrow e + Cl_2(v1)$	$4.35\times10^{-10} T_e^{-1.48} \exp(-0.76/T_e)$	0.07	[19,20]
9	$e + Cl_2 \rightarrow e + Cl_2(v2)$	$8.10\times10^{-11} T_e^{-1.48} \exp(-0.68/T_e)$	0.14	[19,20]
10	$e + Cl_2 \rightarrow e + Cl_2(v3)$	$2.39\times10^{-11} T_e^{-1.49} \exp(-0.64/T_e)$	0.21	[19,20]
11	$e + Cl_2(v1) \rightarrow e + Cl_2(v2)$	$1.04\times10^{-9} T_e^{-1.48} \exp(-0.73/T_e)$	0.07	[19,20]
12	$e + Cl_2(v1) \rightarrow e + Cl_2(v3)$	$2.98\times10^{-10} T_e^{-1.48} \exp(-0.67/T_e)$	0.14	[19,20]
13	$e + Cl_2(v2) \rightarrow e + Cl_2(v3)$	$1.04\times10^{-9} T_e^{-1.48} \exp(-0.73/T_e)$	0.07	[19,20]
14	$e + Cl_2 \rightarrow 2Cl + e$	$6.67\times10^{-8} T_e^{-0.1} \exp(-8.67/T_e)$	4	[19,20]
15	$e + Cl_2 \rightarrow Cl_2^{+} + 2e$	$4.87\times10^{-8} T_e^{0.5} \exp(-12.17/T_e)$	11.5	[19,20]
16	$e + Cl_2 \rightarrow Cl + Cl^{+} + 2e$	$1.79\times10^{-7} \exp(-24.88/T_e)$	14.25	[19,20]
17	$e + Cl_2 \rightarrow 2Cl^{+} + 3e$	$1.46\times10^{-10} T_e^{2.16} \exp(-21.42/T_e)$	28.5	[19,20]
18	$e + Cl_2 \rightarrow Cl^{+} + Cl^{-} + e$	$3.45\times10^{-10} T_e^{0.13} \exp(-19.7/T_e)$	14.25	[19,20]
19	$e + Cl_2 \rightarrow Cl + Cl^{-}$	$\left(22.5 T_e^{-0.46} e^{-2.82/T_e} - 12.1 e^{-0.99/T_e} + 6.54\right)\times10^{-10}$	0	[19,20]
20	$e + Cl_2(v1) \rightarrow Cl + Cl^{-}$	$\left(9.29 T_e^{-0.47} e^{-2.83/T_e} - 4.96 e^{-0.99/T_e} + 2.7\right)\times10^{-9}$	0	[19,20]

21	$e + Cl_2(v2) \rightarrow Cl + Cl^-$	$\begin{pmatrix} 20.1T_e^{-0.47} e^{-2.83/T_e} \\ -10.8e^{-0.97/T_e} + 5.92 \end{pmatrix} \times 10^{-9}$	0	[19,20]
22	$e + Cl_2(v3) \rightarrow Cl + Cl^-$	$\begin{pmatrix} 30.5T_e^{-0.46} e^{-2.82/T_e} \\ -16.3e^{-0.99/T_e} + 8.81 \end{pmatrix} \times 10^{-9}$	0	[19,20]
23	$e + Cl \rightarrow Cl^+ + 2e$	$2.48 \times 10^{-8} T_e^{0.62} \exp(-12.76/T_e)$	14.25	[19,20]
24	$e + Cl^- \rightarrow Cl + 2e$	$2.33 \times 10^{-15} T_e^{1.45} \exp(-2.48/T_e)$	2.36	[19,20]
25	$e + Cl^- \rightarrow Cl^+ + 3e$	$3.38 \times 10^{-9} T_e^{0.75} \exp(-25.28/T_e)$	16.61	[19,20]
26	$e + Cl_2^+ \rightarrow 2Cl$	$9.0 \times 10^{-8} T_e^{-0.5}$	-11.5	[19,20]
27	$Ar^m + Ar^m \rightarrow e + Ar + Ar^+$	6.2×10^{-10}	0	[19,20]
28	$Ar^m + Ar \rightarrow Ar + Ar$	3.0×10^{-15}	0	[19,20]
29	$Cl_2^+ + Cl^- \rightarrow 3Cl$	$5.0 \times 10^{-8} \left(300/T_g\right)^{0.5}$	0	[19,20]
30	$Cl_2^+ + Cl^- \rightarrow Cl + Cl_2$	$5.0 \times 10^{-8} \left(300/T_g\right)^{0.5}$	0	[19,20]
31	$Cl^+ + Cl^- \rightarrow 2Cl$	$5.0 \times 10^{-8} \left(300/T_g\right)^{0.5}$	0	[19,20]
32	$Cl^+ + Cl_2 \rightarrow Cl + Cl_2^+$	5.4×10^{-10}	0	[19,20]
33	$2Cl + Cl_2 \rightarrow Cl_2 + Cl_2$	$3.5 \times 10^{-39} \exp\left(810/T_g\right)$	0	[19,20]
34	$2Cl + Cl \rightarrow Cl_2 + Cl$	$8.75 \times 10^{-40} \exp\left(810/T_g\right)$	0	[19,20]
35	$Cl_2 + Ar^+ \rightarrow Cl_2^+ + Ar$	1.9×10^{-10}	0	[19,20]
36	$Cl_2 + Ar^+ \rightarrow Cl + Cl^+ + Ar$	5.7×10^{-10}	0	[19,20]
37	$Cl^- + Ar^+ \rightarrow Cl + Ar$	$5.0 \times 10^{-8} \left(300/T_g\right)^{0.5}$	0	[19,20]

38	$Cl_2 + Ar^m \rightarrow Cl_2^+ + Ar + e$	7.1×10^{-10}	0	[19,20]
39	$Cl + Ar^+ \rightarrow Cl^+ + Ar$	2.0×10^{-10}	0	[19,20]
40	$2Cl + Ar \rightarrow Cl_2 + Ar$	$8.75\times10^{-40}\exp\left(-810/T_g\right)$	0	[19,20]
41	$2Cl + Ar^m \rightarrow Cl_2 + Ar$	$8.75\times10^{-40}\exp\left(-810/T_g\right)$	0	[19,20]

Table 1: Chemical reaction set considered in the model
[a]The unit of the rate coefficient is $cm^3\ s^{-1}$.
[b]v1, v2, v3 represent different vibrational excited states.

No.	Surface reaction	Sticking coefficient	Ref.
1	$Cl_2(v1) + wall \rightarrow Cl_2$	1	[19,20]
2	$Cl_2(v2) + wall \rightarrow Cl_2$	1	[19,20]
3	$Cl_2(v3) + wall \rightarrow Cl_2$	1	[19,20]
4	$Cl_2^+ + wall \rightarrow Cl_2$	1	[19,20]
5	$Cl^+ + wall \rightarrow Cl$	1	[19,20]
6	$Cl + wall \rightarrow 1/2\,Cl_2$	0.04	[21]
7	$Ar^+ + wall \rightarrow Ar$	1	[19,20]
8	$Ar^m + wall \rightarrow Ar$	1	[19,20]

Table 2: Surface reaction set considered in the model

III. Results and discussion

In this section, the discharge structures as adjusting cyclically the certain discharge parameters, pressure and reactive gas ratio, are presented and the behind physics for the different profiles, such as the density, potential, chemical source, net charge density, and drift terms etc., are analysed theoretically. For better understanding the workflow of cyclic adjustment of discharge parameters, the catalogue of this section is first given below.

III.a) Increasing Cl_2 content at low pressures, e.g., 10mTorr, from 5% Cl_2 content

i) Species-stratification, quasi-delta anion and self-coagulation

As the early analytic work predicted, there are two types of discharge stratification in the electronegative plasmas. Here in this section, the known species-stratification is illustrated, which occurs at the case of low electronegativity. It indicates that the densities of different charged species in the electronegative core is stratified [8]. This is different with the so-called space-stratification that divides the whole bulk discharge region into the electronegative core and electropositive edge [9]. The fluid simulation shown in Figure 1 gives the Cl- anion density and its net source, as well as the summed cations density and electron density, at only 5% Cl_2 content in the feedstock gas mixture. As seen, the Cl^- density behaves like a comet, also called as the quasi-delta profile. The novel anion density profile has been reported in our previous paper [17] about the Ar/O_2 inductively coupled plasma, which is in the case of low electronegativity case as well. As reported in Ref. [17], the comet profile of anion is formed by the self-coagulation behaviour controlled by a quasi- Helmholtz equation. Self-coagulation we reported is a type of self-organization. It happens naturally once the needed conditions are satisfied, negative

chemical source and transport component of free diffusion. Superficially, the self-consistent fluid simulation predicts a delta profile, which is not in accord to the analytic solution that gives the smooth species-stratified density profiles. Nevertheless, when zooming into the delta inside, it is found that species-stratification is hidden by the delta structure as shown in Figure 2. As seen, after a set of operations of expansion, normalization and plotting format revision, the fluid simulation perfectly repeats the analytic prediction in the scope of species-stratification. In the simulation, why the delta structure is superposed? Caused by the anion dynamics (described above). The anion is assumed to satisfy the Boltzmann relation in the analytics and the self-organization cannot be considered. Although the simulation is more complete, the importance of analytic work predictions is emphasized, since it is difficult to understand the simulations without the guide of analytics.

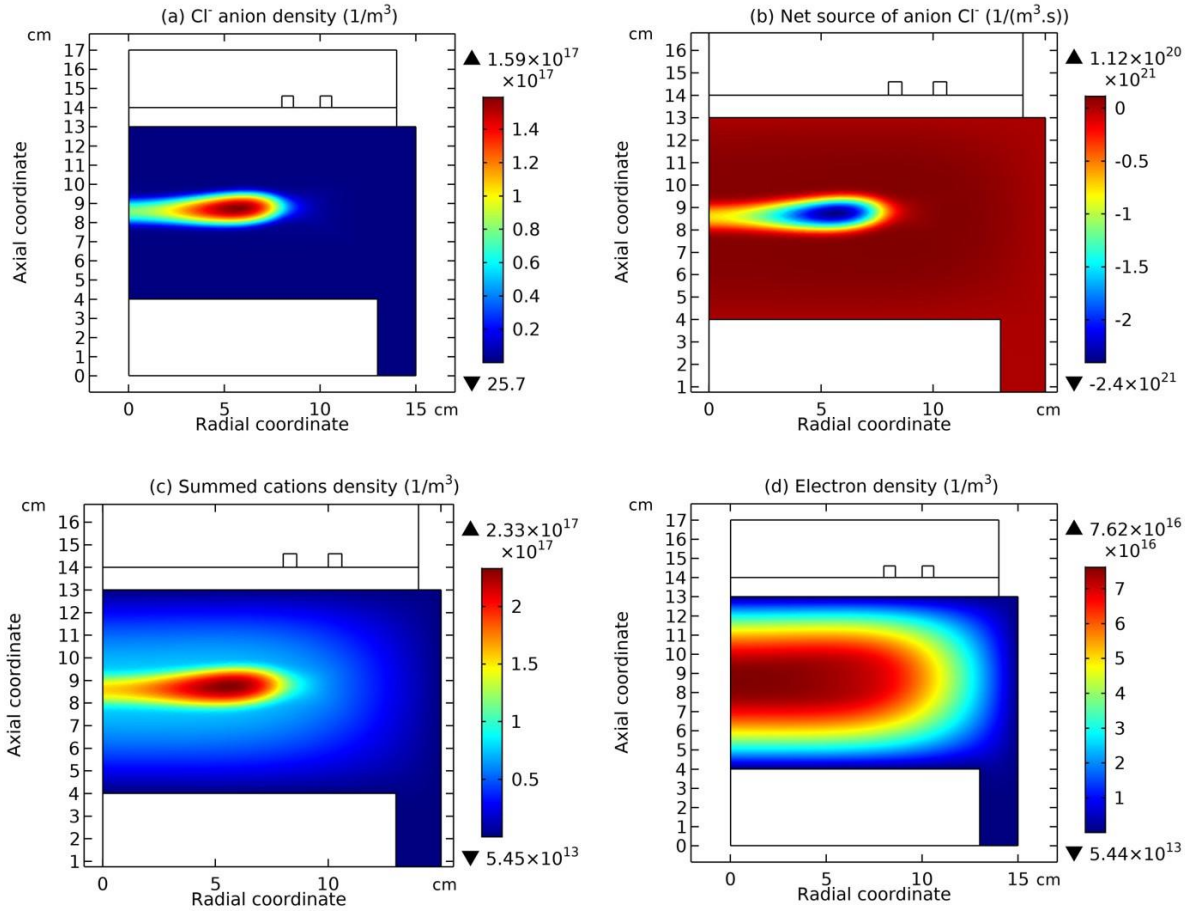

Figure 1: Cl^- anion density (a), the net source of Cl^- (b), summed cations density (c) and electron density (d) in the Ar/Cl_2 inductively coupled plasma, given by the fluid simulation at the discharge conditions of 300W, 10mTorr and 5% of Cl_2 gas content.

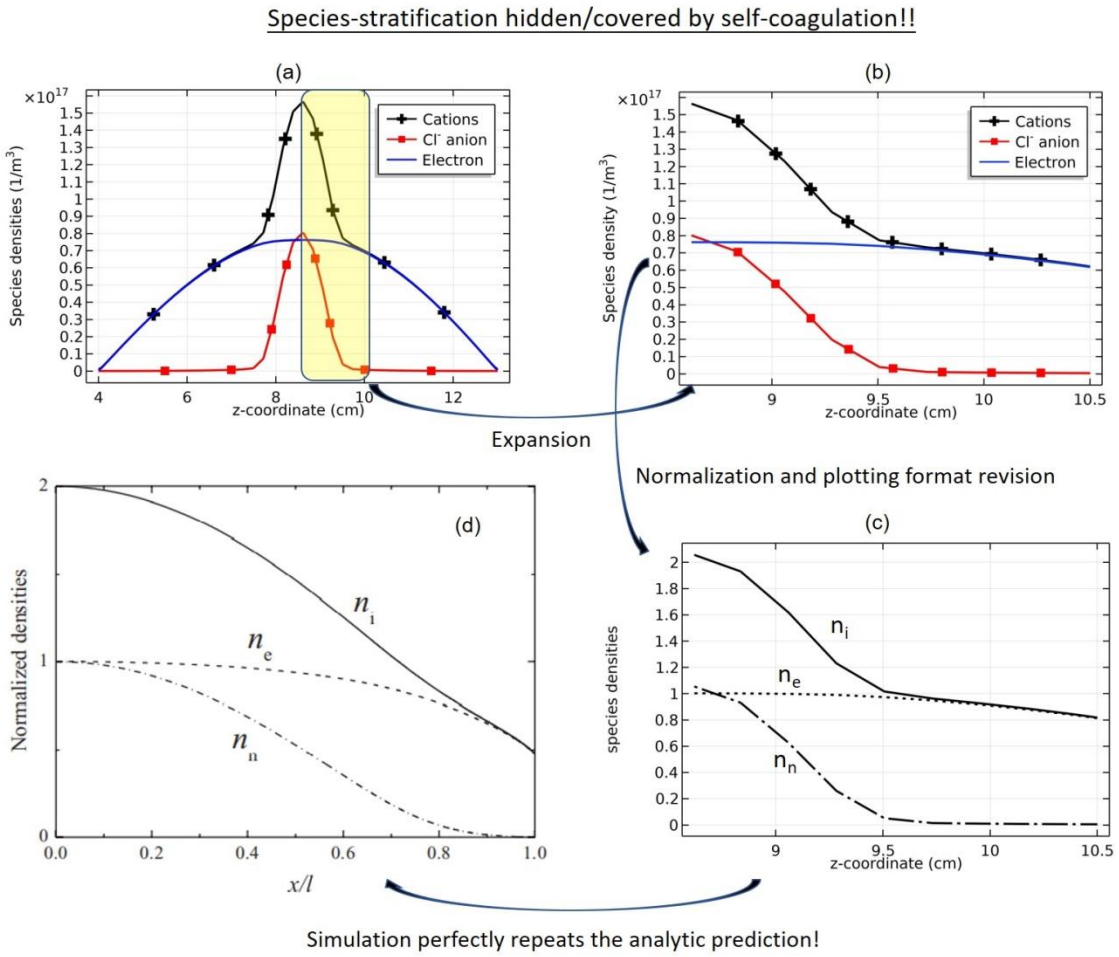

Figure 2: (a) Simulated axial profiles of different species densities in the Ar/Cl_2 inductively coupled plasma, along the reactor axis, (b) the expanded part of these axial profiles inside the half delta structure, (c) still these expanded profiles but plotted in a different format and meanwhile normalized, and (d) sampled species density profiles of analytic solution that ignores the anion dynamics in Ref. [8]. The simulation is given by the fluid model at the discharge conditions of 300W, 10mTorr and 5% Cl_2 content. This plot shows that the species-stratification is hidden by the self-coagulation behaviour.

III.b) Conventional space-stratification analogous to Ar/SF_6 discharge

As increasing the Cl_2 content ratio up to, e.g., 90%, at the low pressure of 10mTorr, the discharge structure of Ar/Cl_2 inductively coupled plasma evolves to the conventional space-stratification, an electronegative core and an electropositive edge, as seen from Fig. 3. Fig. 4 plots the axial and radial distributions of species densities, accordingly. As seen, this is very similar to the Ar/SF_6 inductively coupled discharge case, where the parabola trait of core [6, 7] and the self-coagulation portion along the radial profile are captured, as seen from Figs. 5 and 6. The difference is that the Ar/Cl_2 plasma electronegativity is weaker than the Ar/SF_6 plasma, and hence the reactive gas content of Ar/Cl_2 plasma, 90%, is higher than the Ar/SF_6 case, 10%. As seen next, even at the high reactive gas ratio, the electronegativity of Ar/Cl_2 plasma is significantly lower than the Ar/SF_6 plasma (see Fig. 12 for reference). Accordingly, the electropositive halo region of Ar/Cl_2 plasma is wider and the core electron density is higher, as compared to the Ar/SF_6 plasma in Figs. 5 and 6, which is again in accord to the analytic prediction of Ref. [7].

It is stressed that the space-stratification discovered here in the electronegative and radio frequency (RF) plasma sources is different with the striation that is discovered in the direct current (DC) glow discharge [27]. The stratification specific to the electronegative ICPs is meant that the whole discharge area is divided into two regions, i.e., the centric electronegative core that consists mainly of the cations and anions with less electrons and the peripherical electropositive edge that consists purely of the cations and electrons, without the anions, as

previously reported in Refs. [28-32]. The core plasma is electronegative plasma and the peripheric plasma is electropositive plasma, at the interface of which is dominated by the double layer [33-36]. This is different with the striation discovered in the DC glow discharges that consists of alternating bright and dark areas, which is spatially cyclic. In a word, these are two different phenomena existing in the plasma.

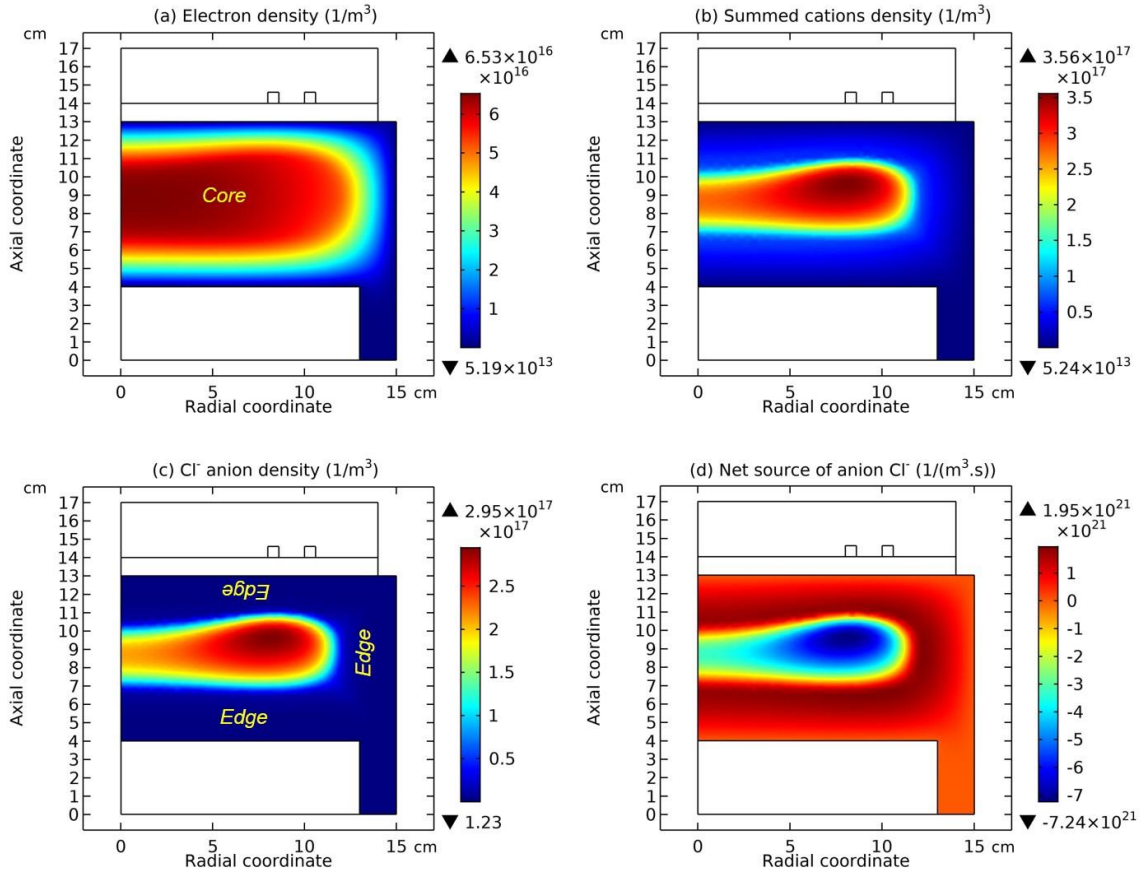

Figure 3: Electron density (a), summed cations density (b), Cl^- anion density (c), and its net source (d) of Ar/Cl_2 inductively coupled plasma given by the fluid simulation at the discharge conditions of 300W, 10mTorr and 90% Cl_2 content.

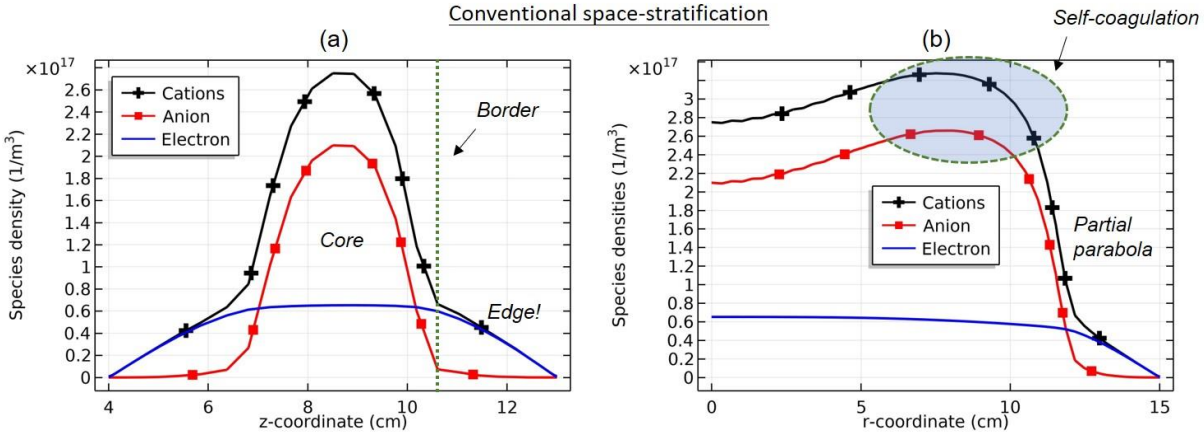

Figure 4: Axial (a) and radial (b) profiles of species densities of Ar/Cl_2 inductively coupled plasma given by the fluid simulation at the discharge conditions of 300W, 10mTorr and 90% Cl_2 content. The figure exhibits the conventional space-stratification macro-profile and the self-coagulation structure contained in the core.

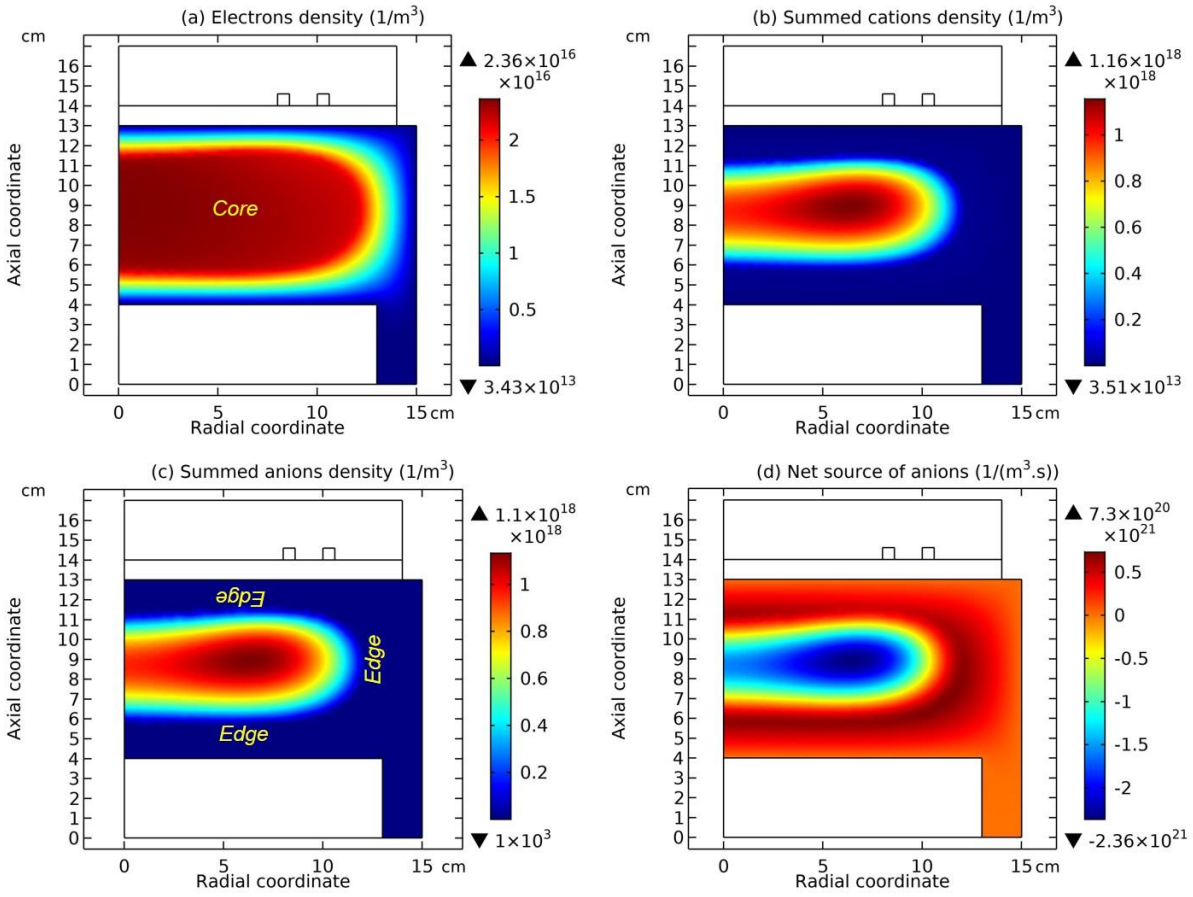

Figure 5: Electrons density (a), summed cations density (b), summed anions density (c), and the net source of anions (d) in Ar/SF_6 inductively coupled plasma given by the fluid simulation at the discharge conditions of 300W, 10mTorr and 10% SF_6 content.

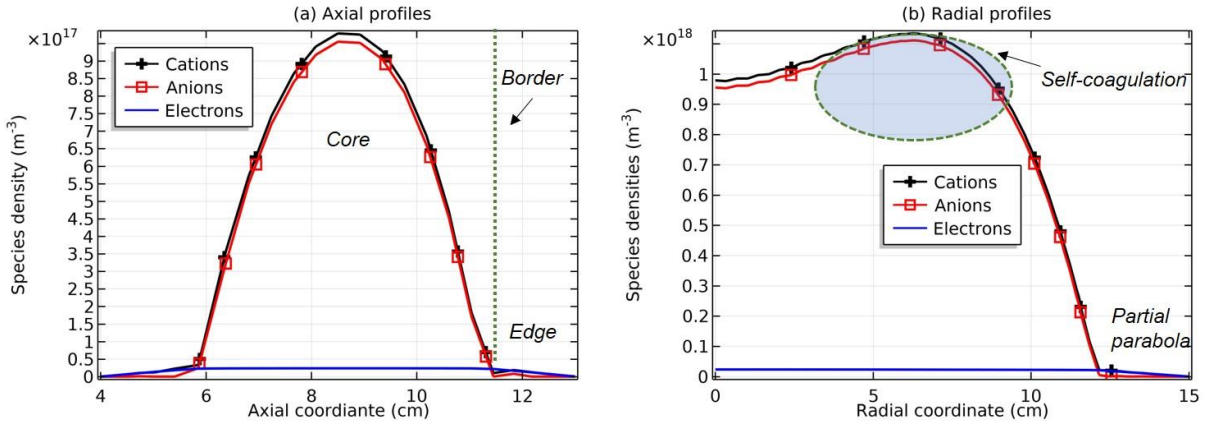

Figure 6: Axial (a) and radial (b) profiles of species densities of Ar/SF_6 inductively coupled plasma given by the fluid simulation at the discharge conditions of 300W, 10mTorr and 10% SF_6 content. They show the space-stratification macro-profile and the self-coagulation structure of core in the Ar/SF_6 plasma, which is similar to the Ar/Cl_2 plasma case.

III.c) From delta/comet profile to parabola and the core expansion: Cl_2 gas content effect

The simulation shows at 10mTorr the comet profile of Ar/Cl_2 inductively coupled plasma evolves into the parabola profile upon increasing the Cl_2 gas ratio, as shown in Fig. 7.

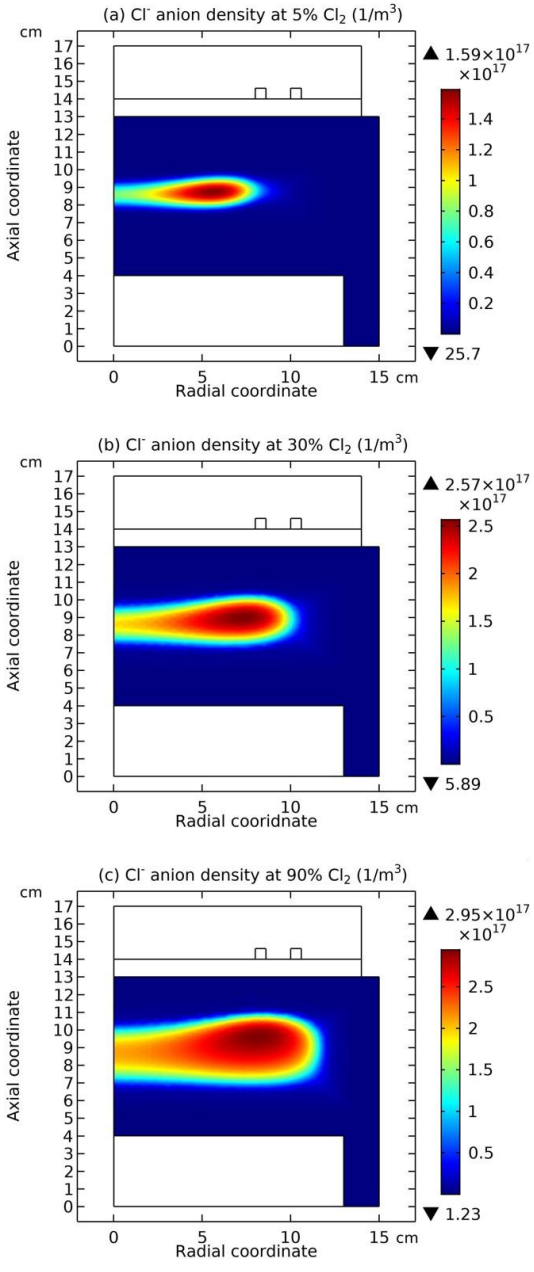

Figure 7: Cl^- anion density at (a) 5%, (b) 30% and (c) 90% Cl_2 contents, given by the fluid simulation of Ar/Cl_2 inductively coupled plasma at the low pressure, 10mTorr, and the power of 300W. The plot shows the evolution of delta profile to the parabola profile, against increasing the reactive gas ratio.

At low Cl_2 content, the delta profile is specific space-stratification structure at the extreme condition of a very low electronegativity, in which the electronegative core is shrunk. This is logic and determined by the origin of space-stratification [6, 7]. It is noted the self-coagulation is accompanied in the above cases. The difference is that at low Cl2 content, electronegative core is slim and self-coagulation is predominant; and so, anion displays the comet profile. While at high Cl_2 content, core is fat and self-coagulation is more squeezed in the centre of wide parabola. As seen next, the slim and fat cores lead to the blue sheath and double layer, respectively, at the interface of core and edge.

III.d) Increasing the pressure at high Cl_2 contents, e.g., 90%, from 10mTorr

i) Evolution of ions density profile from parabola to flat-top, besides for self-coagulation-to-coil (SCC) scheme

In Fig. 8(a-d), the evolution of Cl^- anion density with pressure is presented at fixed Cl_2 content, 90%, and 300W. Besides for the self-coagulation-to-coil (SCC) behaviour, it experiences the parabola, ellipse and flat-top models, which is well known to be determined by the respective analytic theory in Refs. [6, 7]. The cations density exhibits the same trend with pressure as the anions, given by the gentle ambi-polar self-coagulation of ions as reported here in Fig. 8(e,f) that does not destroy the ambi-polar diffusion potential barrel (see the next Secs. (b, c) for more details). This is different with the Ar/SF_6 inductively coupled plasma that holds the similar macro-discharge structure, but at the rather high electronegativity. As seen, the ambi-polar self-coagulation of ions in the Ar/SF_6 inductively coupled plasma is advective, hence giving rise to the blue sheath at the interface of core and edge as reported in Ref. [16], after the ambi-polar diffusion potential collapses.

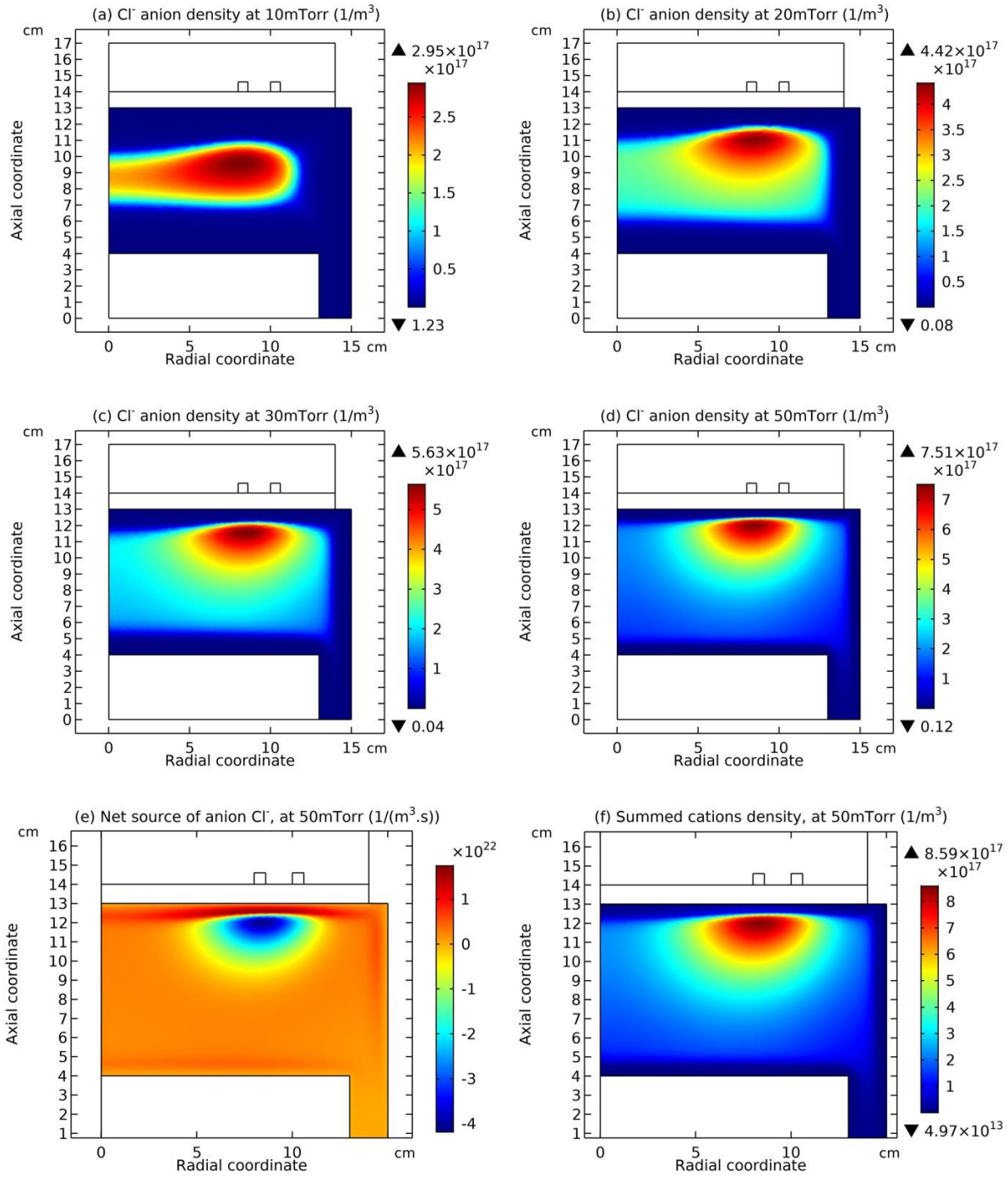

Figure 8: Cl^- anion density at (a) 10mTorr, (b) 20mTorr, (c) 30mTorr and (d) 50mTorr, at 90% Cl_2 content and 300W, given by the fluid simulation of Ar/Cl_2 inductively coupled plasma at the fixed chlorine content, 90%, and the power of 300W. For clearly showing the ambi-polar self-coagulation of ions at 50mTorr and 90% Cl_2 content, the negative net source of anion, Cl^-, in Panel (e) and the summed cations density in Panel (f) with the similar profile as the anion in Panel (d) are shown.

ii) Electron coagulates at ambi-polar diffusion of electrons and ions self-coagulation

In Fig. 9, the electron density coagulates toward the coil at increasing the pressure because of the ions self-coagulation, at 90% Cl_2 content and 300W power, very similar to the Ar/SF_6 plasma; see Fig. 11(a, d) for reference. The difference is that the ambi-polar diffusion potential barrels of the Ar/Cl_2 plasmas at 50mTorr and 90mTorr are not collapsed, as shown in Fig. 10(b, e), while the potential barrels of the Ar/SF_6 plasmas at 50mTorr and 90mTorr are collapsed, as shown in Fig. 11(b, e), due to the different electronegativities of two types of plasm shown

in Fig. 12. Since the Ar/Cl_2 plasmas at 50mTorr and 90mTorr are still in the scope of ambi-polar diffusion potential, the peripherical self-coagulations of electrons in Ar/SF_6 plasma by referring to the negative net sources of electrons in Fig. 13(c, d) and reported in Ref. [16] are not happened due to the lack of free diffusion, although the negative net sources of electrons in the peripheric regions of Ar/Cl_2 plasmas form in Fig. 13(a, b). Hence, the electrons of Ar/Cl_2 plasma at 50mTorr and 90mTorr are more or less Boltzmann balanced in Fig. 10(c, f), different with the electrons of Ar/SF_6 plasma in Fig. 11(c, f) where the Boltzmann relations are clearly deviated. It is seen the central self-coagulation of ions leads to the tight coagulation of electrons to the coil and the peripherical self-coagulation of electron significantly deviates its Boltzmann relation therein. As seen next, at the high pressure of 90mTorr, when decreasing the Cl_2 content up to 5%, this tight-coagulation-to-coil of electrons, which is specific to the electronegative plasma with its density peak almost attached to the dielectric window, will be replaced by the type of departing-coil-type coagulation, where the anion self-coagulation is destroyed at the shortage of reactive feedstock. See the Fig. 27 of Sec. (3.3) for more details.

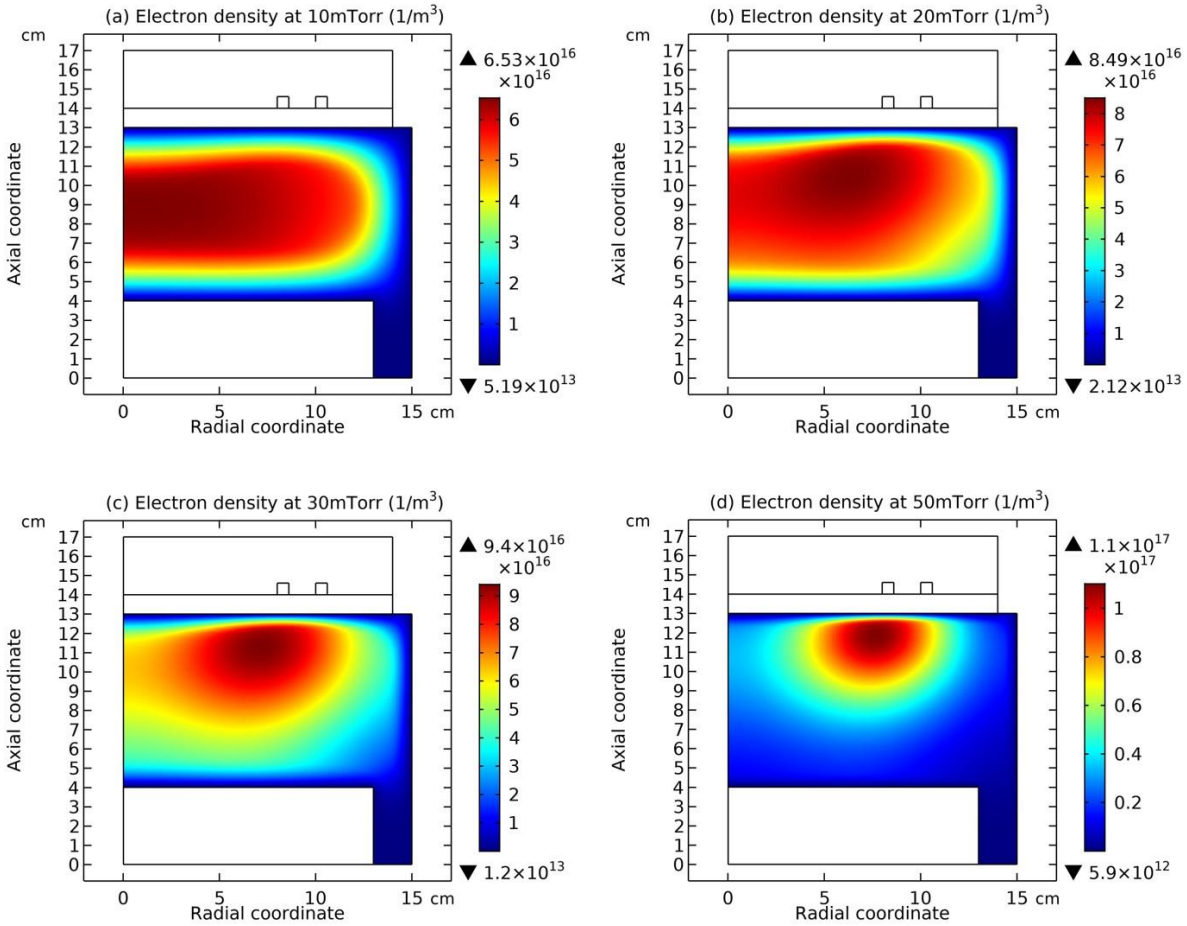

Figure 9: Electron density profiles of Ar/Cl_2 inductively coupled plasma at different pressures, (a) 10mTorr, (b) 20mTorr, (c) 30mTorr, and (d) 50mTorr, given by fluid simulation at 300W and 90% Cl_2 content.

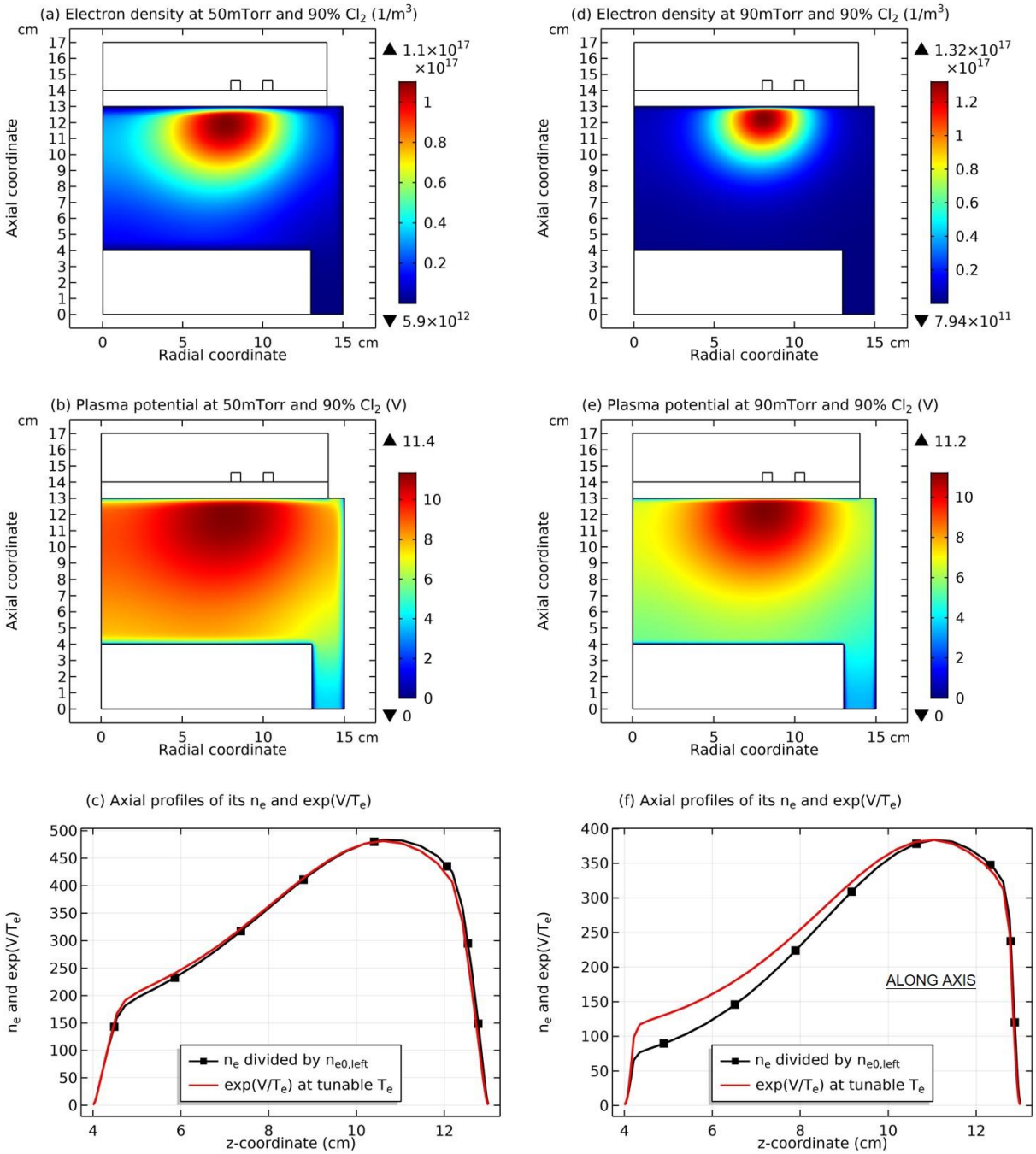

Figure 10: Electron density (a), plasma potential (b) and its Boltzmann relation (c) of 50mTorr inductively coupled Ar/Cl_2 plasma, and these three quantities (d-f) of 90mTorr inductively coupled Ar/Cl_2 plasma, given by the fluid simulation at 300W and 90% Cl_2 content.

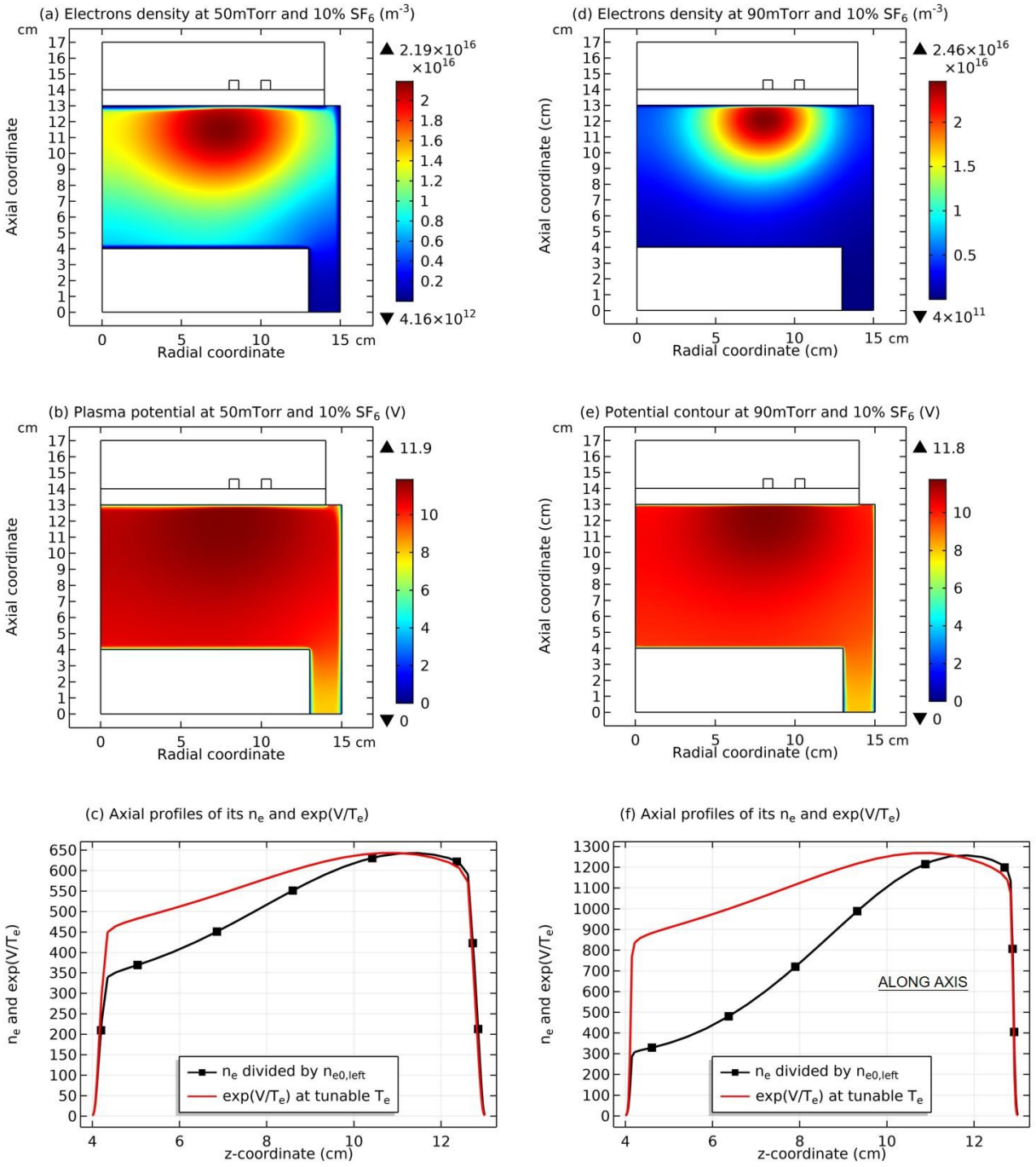

Figure 11: Electron density (a), plasma potential (b) and its non-Boltzmann relation (c) of 50mTorr inductively coupled Ar/SF_6 plasma, and these three quantities (d-f) of 90mTorr inductively coupled Ar/SF_6 plasma, given by the fluid simulation at 300W and 10% SF_6 content.

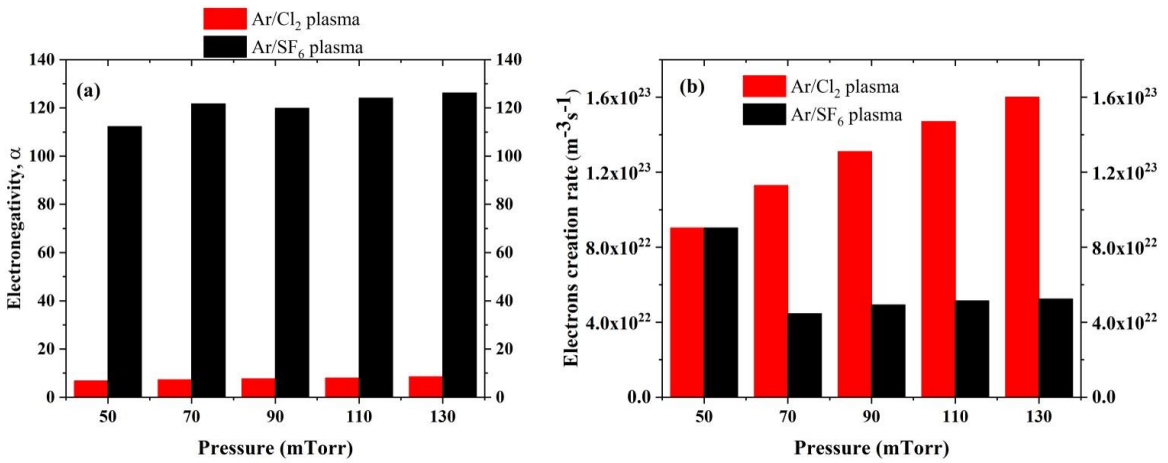

Figure 12: Comparison of electronegativities (a) and electrons creation sources (b) between the Ar/Cl_2 and Ar/SF_6 inductively coupled plasmas, at different pressures. The electronegativity is defined as $\alpha=n_-/n_e$, where n_- and n_e are the maxima of anions density and electron density, respectively. The discharge powers of Ar/Cl_2 and Ar/SF_6 plasmas are both 300W, and the Cl_2 and SF_6 contents in the gas mixtures are 90% and 10%, respectively. The rather high electrons creation rates of Ar/Cl_2 plasmas in Panel (b) leads to their low electronegativities in Panel (a), as compared to the Ar/SF_6 plasma.

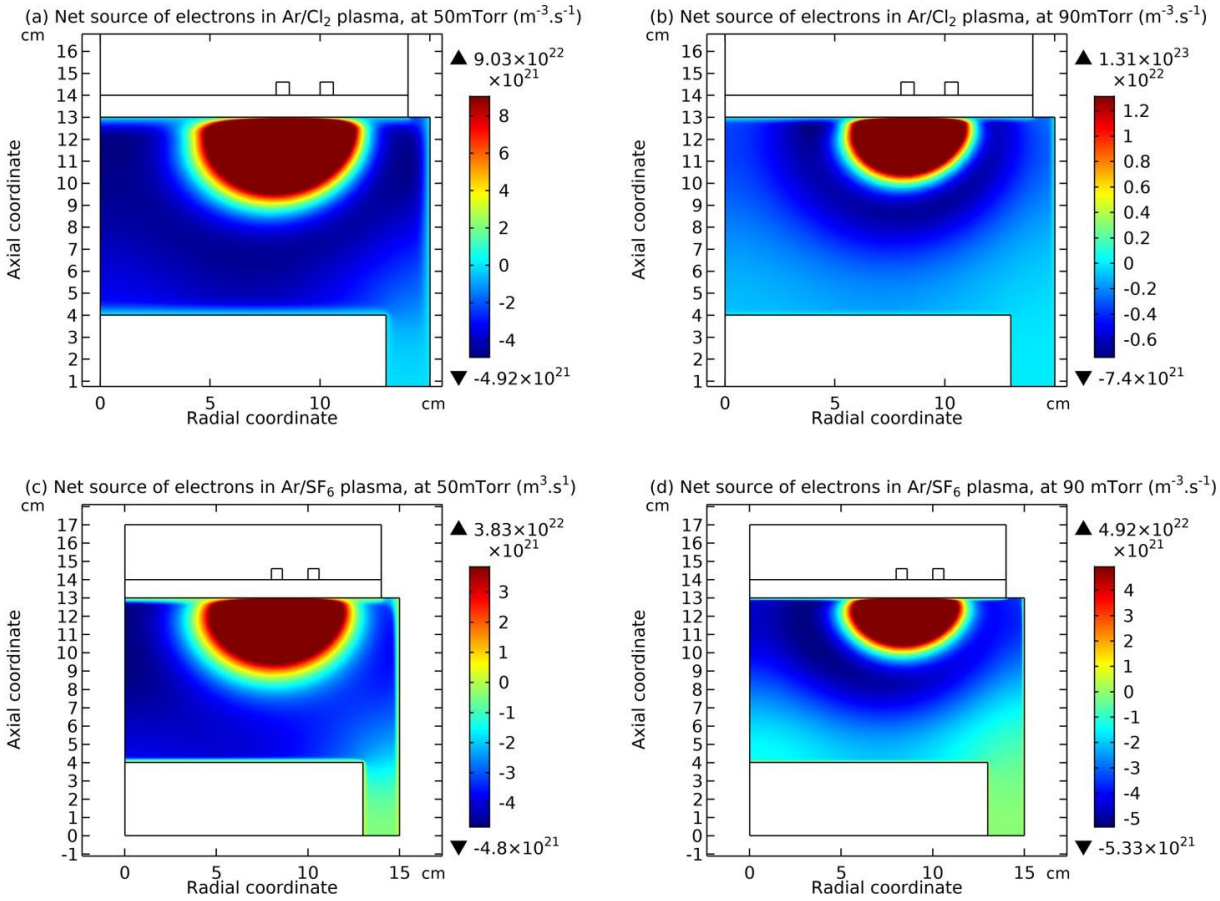

Figure 13: Net source of electrons in Ar/Cl_2 inductively coupled plasma at (a) 50mTorr and (b) 90mTorr, respectively, and the net source of electrons in Ar/SF_6 inductively coupled plasma at (c) 50mTorr and (d) 90mTorr, respectively. It is noted that the maxima in the legends of these figures are truncated to exhibit clearly the negative net source of electrons, away from the heating region under the coil. The discharge powers of Ar/Cl_2 and Ar/SF_6 inductively coupled plasmas are both 300W, and the Cl_2 and SF_6 contents in the gas mixtures are 90% and 10%, respectively.

iii) Ambi-polar diffusion of mediately electronegative plasma that is tolerant to gentle ambi-polar self-coagulation

In this section, the ambi-polar self-coagulation property of Ar/Cl_2 plasma is discussed. In Fig. 14, the net charge densities of different discharge conditions of this plasma are presented. In Fig. 14(a), at 10mTorr and 5% Cl_2 content, where delta type anion is given, the blue and coagulated sheath is seen, which represents the advective ambi-polar self-coagulation, as illustrated in Ref. [16]. The non-advective (i.e., spontaneous) ambi-polar self-coagulation is observed at 10mTorr and 90% Cl2 content, like the case of Ar/SF_6 plasma at 10mTorr and 10% SF_6 content (see Fig. 17(b) for reference).

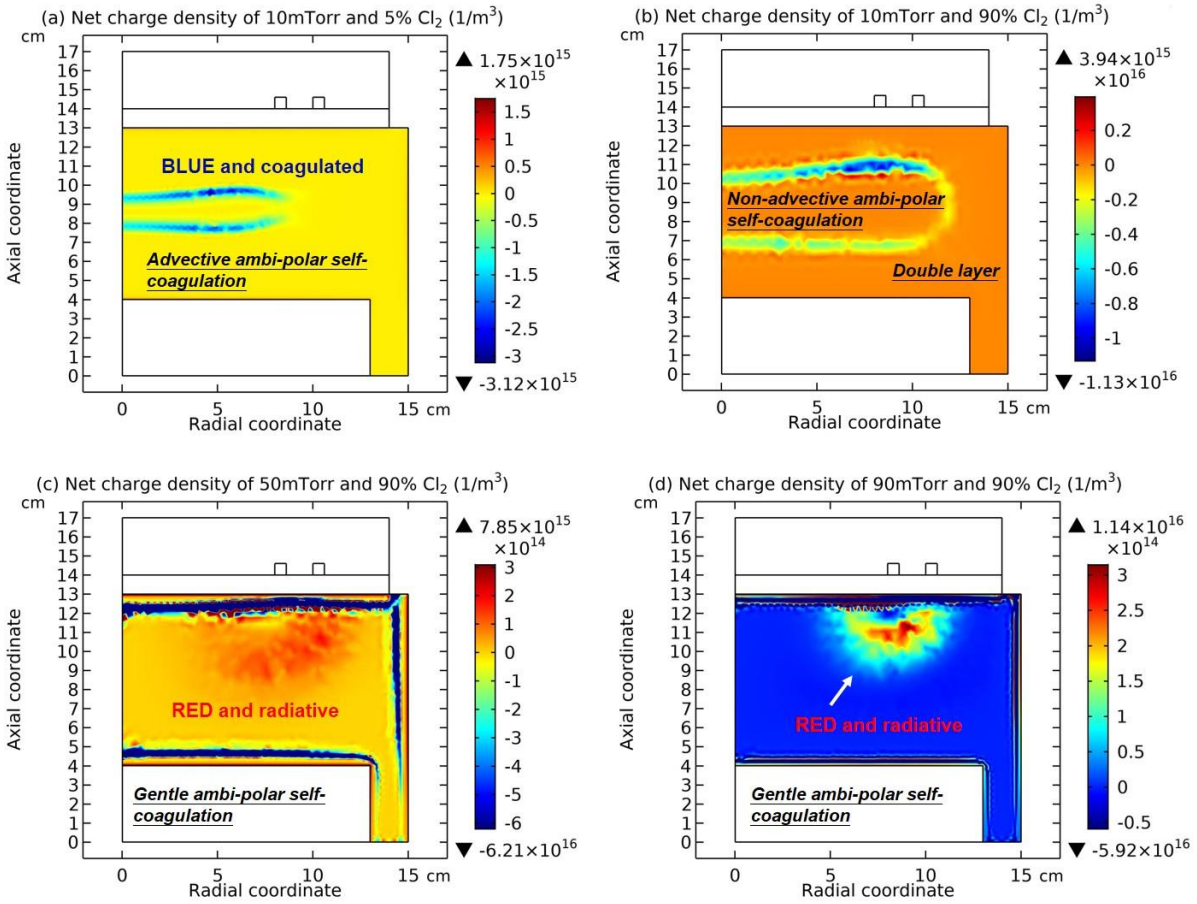

Figure 14: Net charge density of Ar/Cl_2 inductively coupled plasma at (a) 10mTorr and 5% Cl_2 content, (b) 10mTorr and 90% Cl_2 content, (c) 50mTorr and 90% Cl_2 content, and (d) 90mTorr and 90% Cl_2 content, given by the fluid simulations at 300W power.

The double layer, which is another non-electricity type of plasma, appears between the core and edge, and it originates from the fact that the potential in the core collapse as well, as indicated by the flat profile of electrons density in Fig. 3(a) based on the Boltzmann relation. At 50mTorr and 90mTorr of 90% Cl_2 content, it is so strange to find that the blue sheaths are not appeared, which is different with the Ar/SF_6 plasma at similar conditions in Fig. 17(c, d), since the general discharge structures of the two plasmas are so similar, i.e., self-coagulated-to-the coil. It is because the ambi-polar diffusion potential of Ar/Cl_2 plasma are not collapsed as mentioned above and it helps the cations follow the anions self-coagulation, but not forming sheath. This is analogous to the electropositive plasma case where the ions follow the electron diffusion at the ambi-polar diffusion potential, which is approximated electrically neutral. In a word, the process of pure ambi-polar process is known to eliminate the non-neutrality of plasma, applying for both the escaping electrons (via the free diffusion) and the coagulating anions (via the chemical reaction) relative to the cations, as shown in Fig. 15. So, this is called gentle ambi-

polar self-coagulation. The red and radiative sheaths of 50mTorr and 90mTorr cases in Ar/Cl_2 plasmas of Fig. 14(c, d) originate from the mass-point expelling effect, as has been illustrated in Ref. [16].

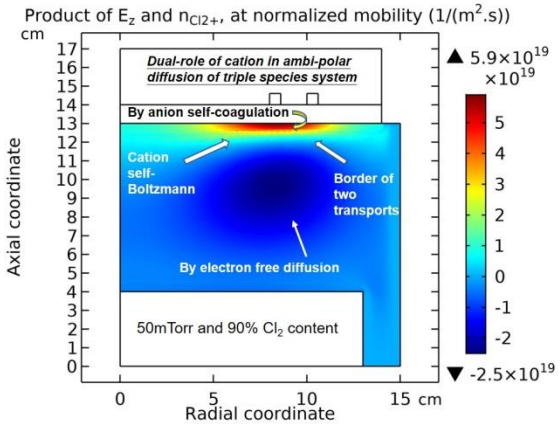

Figure 15: Dual-role of cation in the ambi-polar diffusion of triple species system of plasma, shown by the quantity of axial electric field and Cl_2^+ density product (at normalized mobility) of 50mTorr and 90% Cl_2 content inductively coupled Ar/Cl_2 plasma, given by fluid model simulation at 300W power. The 90mTorr Ar/Cl_2 plasma exhibits the same trend as the 50mTorr case. The product of electric field and cation density represents the drift of it in the ambi-polar diffusion. As the analytic work predicted [5], the drift of ion is the essence of its transport in the process of ambi-polar diffusion of two species system (electron and ion). Other cations, Ar^+ and Cl^+, exhibit the same trend as Cl_2^+. The dual-role of cation in the process is originated from the electron free diffusion and the anion self-coagulation. Axially, free diffusion directs to substrate and self-coagulation directs to dielectric window. So, the drift of cations consists of two parts, thin red part and wide blue part, by referring to the cylindrical coordinate system. At the interface, or the border, of the two transports, the cation drift is almost zero at the counteract of ambi-polar diffusion and self-coagulation, indicating its self-Boltzmann property.

This non-neutrality is not that strong as in Ar/SF_6 plasma, as compared with Fig. 8(d) of Ref. [16], since the coagulated density magnitudes of different cations are not that close to each other, as shown in Fig. 16.

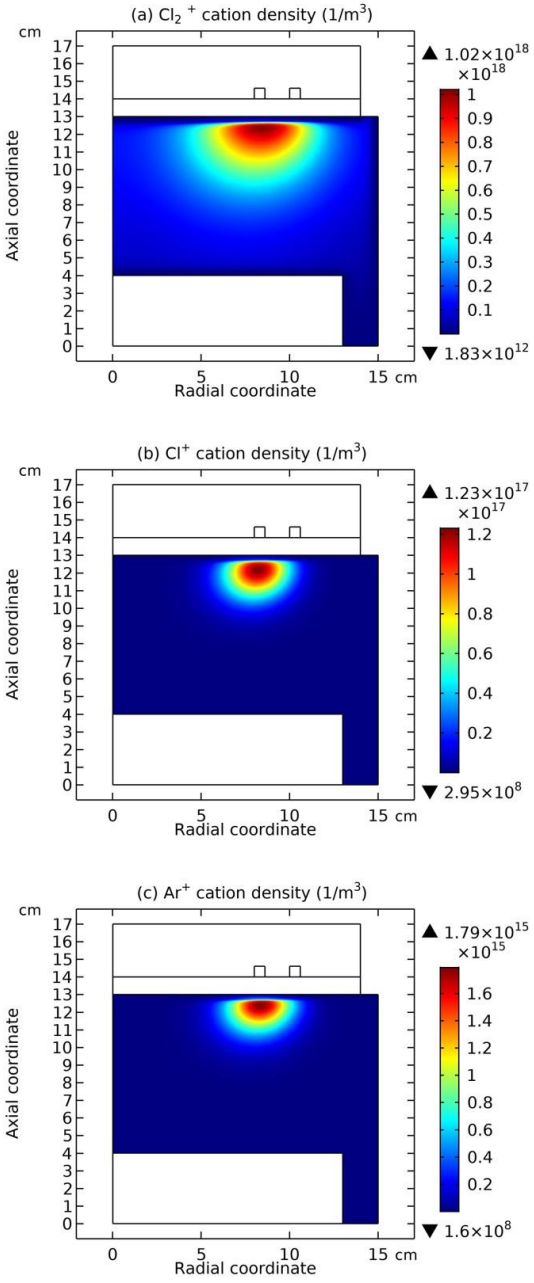

Figure 16: Densities of three types of cation, Cl_2^+, Cl^+ and Ar^+, in the Ar/Cl_2 inductively coupled plasma at 90mTorr and 90% Cl_2 content, given by fluid simulation at 300W.

In Fig. 17(a), the net charge density of Ar/O_2 inductively coupled plasma at 300W, 30mTorr and 10% oxygen content is shown, where the blue sheath is seen to form around the delta anions structure, similar to the case of Ar/Cl_2 inductively coupled plasma at 300W, 10mTorr and 5% chlorine content in Fig. 14(a). The formation of blue and coagulated sheaths around the delta anions structures in the slightly electronegative Ar/Cl_2 and Ar/O_2 plasmas is because there are almost no potential gradients in the locations of deltas, again as indicated by the electrons density profiles in Fig. 1(a) of

present article and directly seen from the potential profile of Fig. 1(d) in Ref. [17]. The formations of blue sheaths under the coil in the Ar/SF_6 inductively coupled plasma at 50mTorr and 90mTorr, is because of the collapse of ambi-polar potential shown in Fig. 11(b,e), which hence is unable to solve the discrepancy led to by the outward ambi-polar diffusion process and the inward ambi-polar self-coagulation process. In a conclusion, the pure ambi-polar potential keeps the electrical neutrality of plasma at the mediate electronegativities, and it more or less collapses and disappears at the cases of the extremely high and low electronegativities, thus leading to many types of internal non-neutralities in the plasma, e.g., blue sheath and double layer.

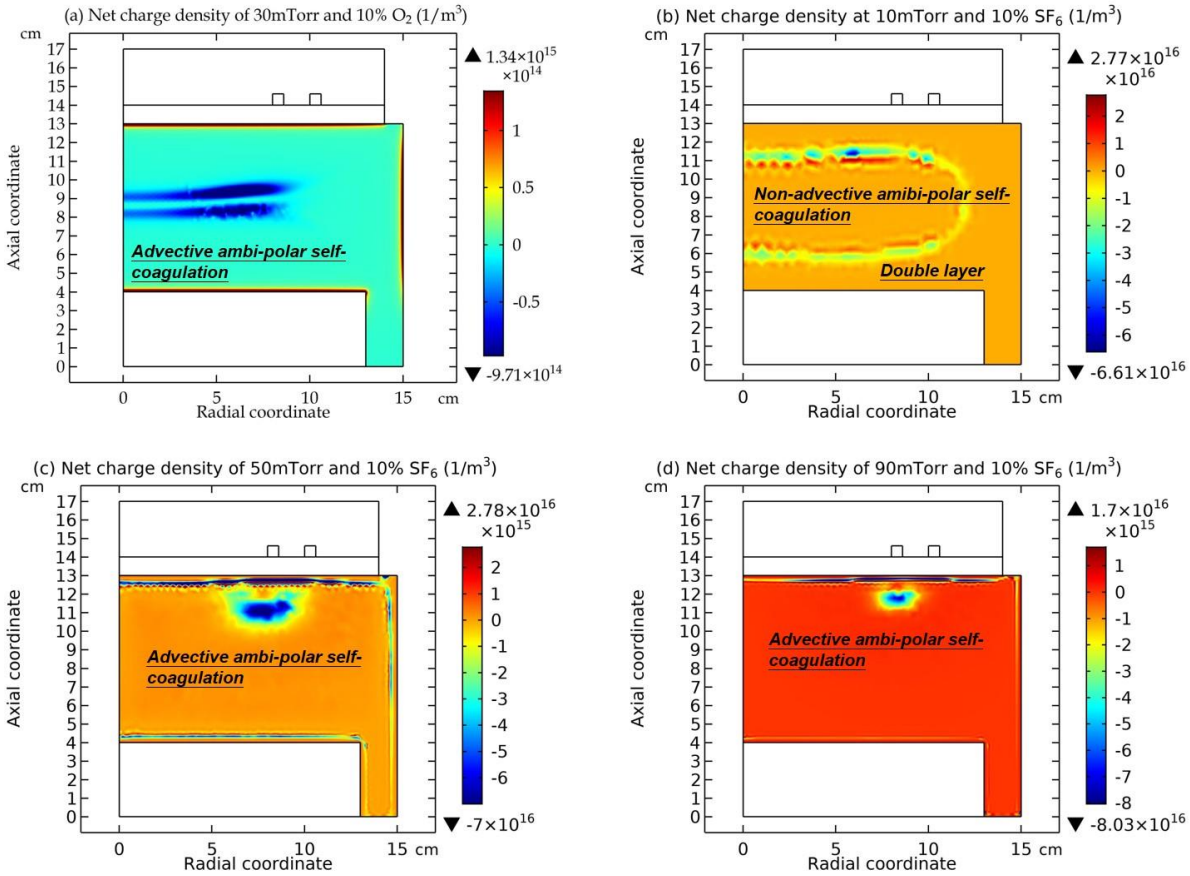

Figure 17: Net charge density of Ar/O_2 inductively coupled plasma at (a) 30mTorr and 10% O_2 content, and the net charge densities of Ar/SF_6 inductively coupled plasma at (b) 10mTorr and 10% SF_6 content, (c) 50mTorr and 10% SF_6 content, and (d) 90mTorr and 10% SF_6 content, given by fluid simulations at the power of 300W. The blue sheath of Panels (c,d) is emphasized in this figure and so the red and radiative non-electricities caused by the coagulated mass-point expelling effect are not shown. Readers may refer to Fig. 8 in Ref. [16], for observing the red and radiative charge density profile of Ar/SF_6 inductively coupled plasma at high pressures, such as 90mTorr.

iv) Non- electric neutralities of plasma, and the collective interaction and against role

Collective role means that the various plasma species interact with each other for finishing certain mission, i.e., a collaboration behaviour. Many instances belong to such type, e.g., chamber border sheath (positive, always plotted red in the colormap). Besides, the advective ambi-polar self-coagulation early reported in Ref. [16] generates electronegative sheath in the plasma bulk, which is plotted as blue in the colormap. On the opposite, against role implies that certain processes of complex plasma fight against each other, and finally give rise to special consequence. For instance, the mass point potential, given by the expelling effect of coagulated density structures with same polarity (originated from self-coagulation), and the double layer, produced by the pushing and accumulating roles of ambi-polar potential of cation and electron on the anions. More details of these plasma non-neutralities are given in Fig. 18.

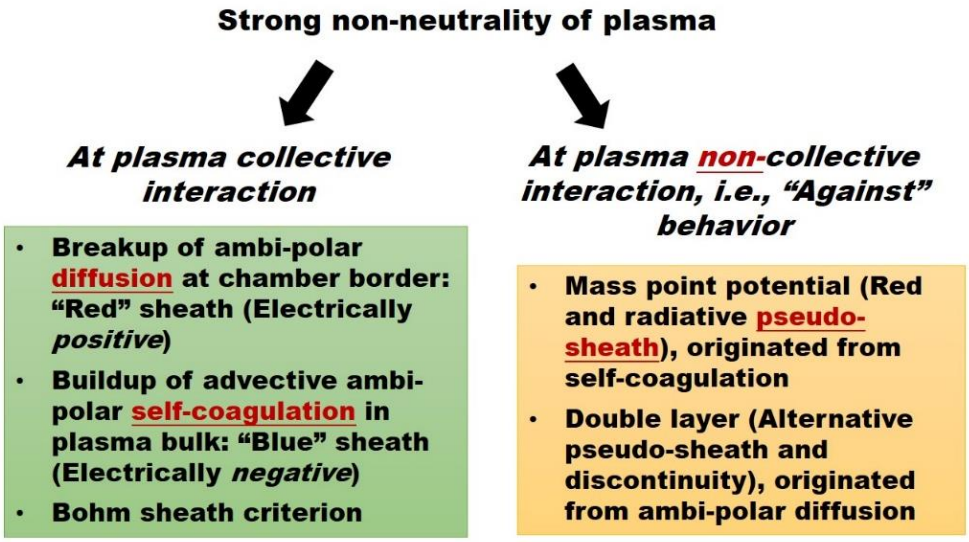

(a) For electropositive plasma and strongly electronegative plasma (*e.g.*, Ar/SF_6 plasma)

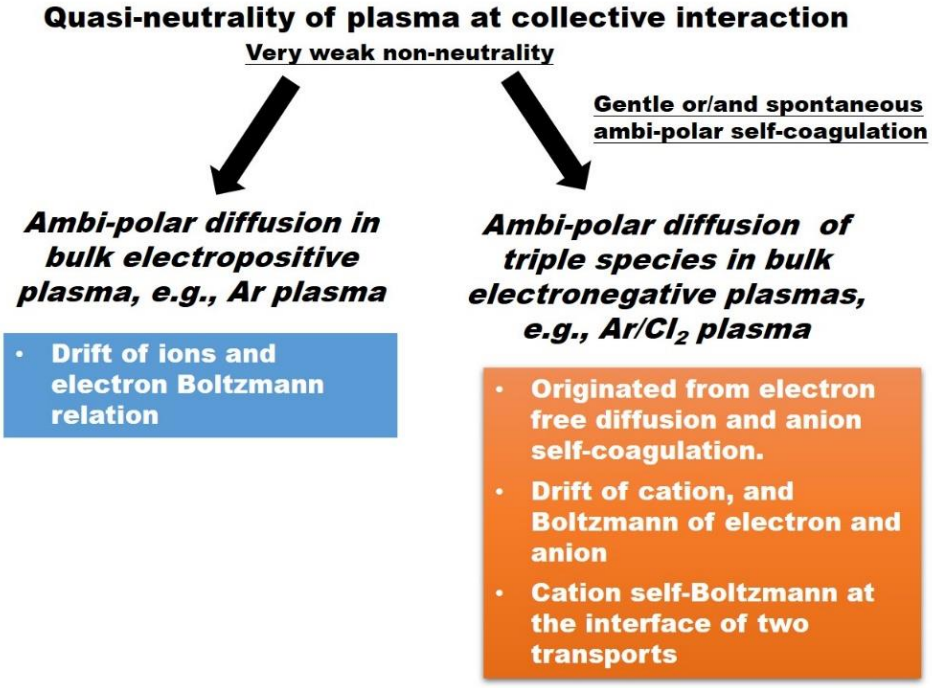

(b) For electropositive plasma and intermediate electronegative plasma

Figure 18: Schematic illustration of plasma non- and quasi- neutralities discovered presently in cold laboratory plasmas.

III.c) Decreasing the Cl_2 content at high pressures, e.g., 90mTorr, from 90% Cl_2 content

i) Collapse of self-coagulation-to-coil

In Fig. 19, the Cl- anion densities at different Cl_2 contents are plotted, at the high pressure of 90mTorr and 300W power of Ar/Cl_2 inductively coupled plasma. It is seen that when decreasing the Cl_2 content, the self-coagulation-to-coil (SCC) phenomenon disappears and the hollow Cl^- anion density is discovered at low enough Cl_2 content, i.e., 5%, in Fig. 19(f).

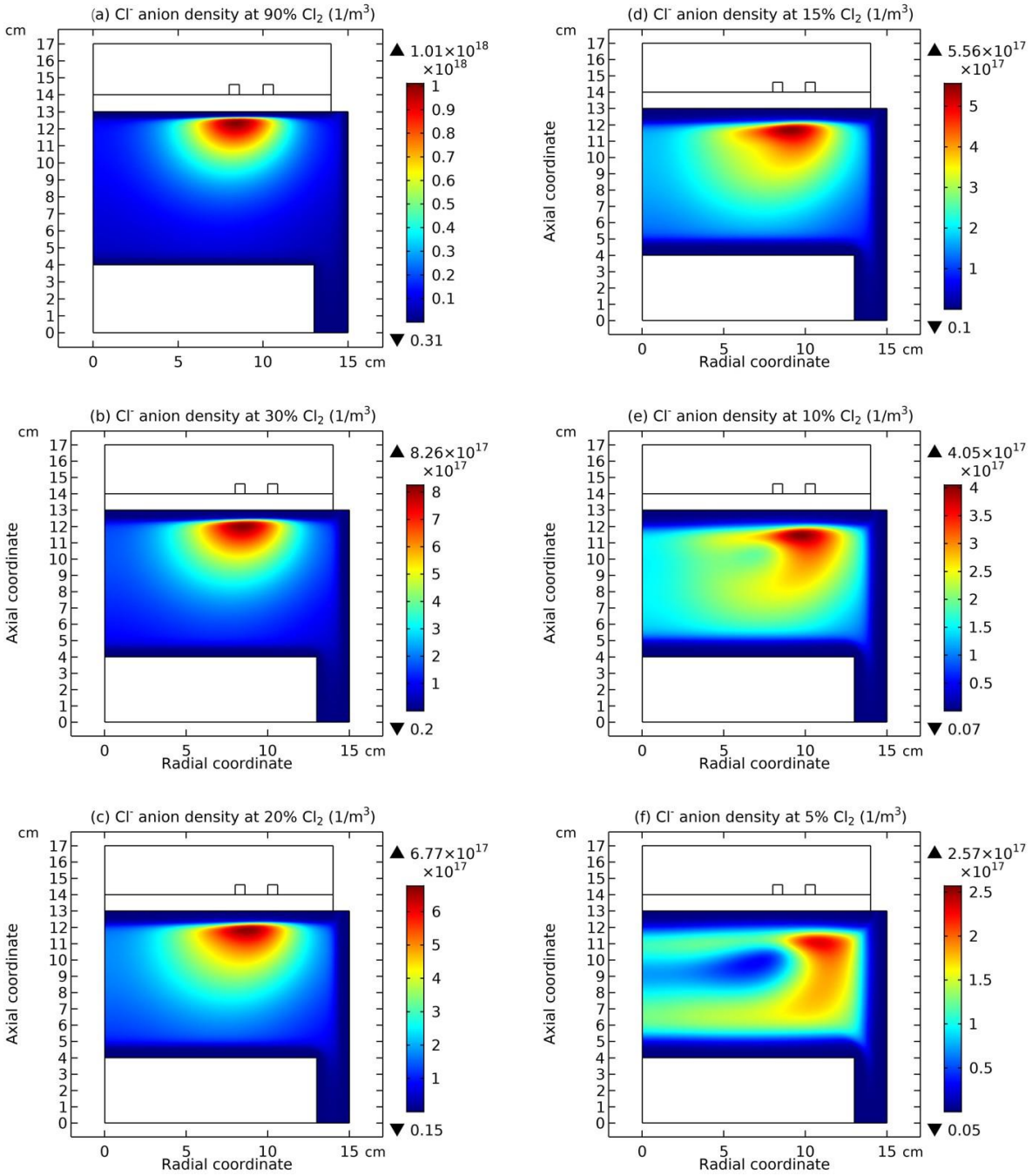

Figure 19: Cl^- anion density of Ar/Cl_2 inductively coupled plasma at (a) 90%, (b) 30%, (c) 20%, (d) 15%, (e) 10%, and (f) 5% Cl_2 contents, given by fluid simulation at 300W and 90mTorr.

ii) Hollow anion density and grouping effect

The hollow anion density profile is more clearly exhibited along the axis in Fig. 20. Moreover, the plasma species are grouped (novel and interesting behaviour) in Fig. 21. Concretely, the electron and the cation pair of Ar^+ and Cl^+ are grouped as their density profiles are the same, coagulated to the coil. Correspondingly, the Cl^- anion and Cl_2^+ cation are grouped, both displaying the hollow density profile. This grouping effect are further demonstrated through the charge density in Fig. 22. In Fig. 22(a) the deduct of electron density from the pair of Ar^+ and Cl^+ is plotted and in Fig. 22(b) the deduct of Cl^- density from the Cl_2^+ is plotted. As compared, they give rise to the charge density profiles with the same distribution but at the opposite polarities. When summed all charged

species, the final net charge density is expressed in Fig. 22(c). The basic double layer structure is more or less seen, which surrounds the weak red positive "charge cloud", defined as grouping potential (one more plasma non-neutrality type).

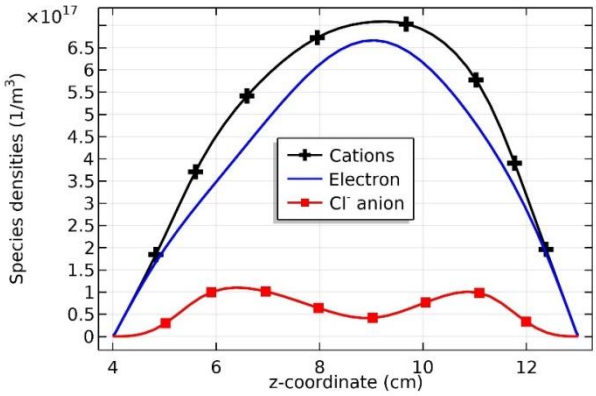

Figure 20: Axial profiles of summed cations, electron and Cl^- anion densities of Ar/Cl_2 inductively coupled plasma, at 5% Cl_2 content and 90mTorr, and 300W, simulated by fluid model. Herein, the hollow anion density is shown.

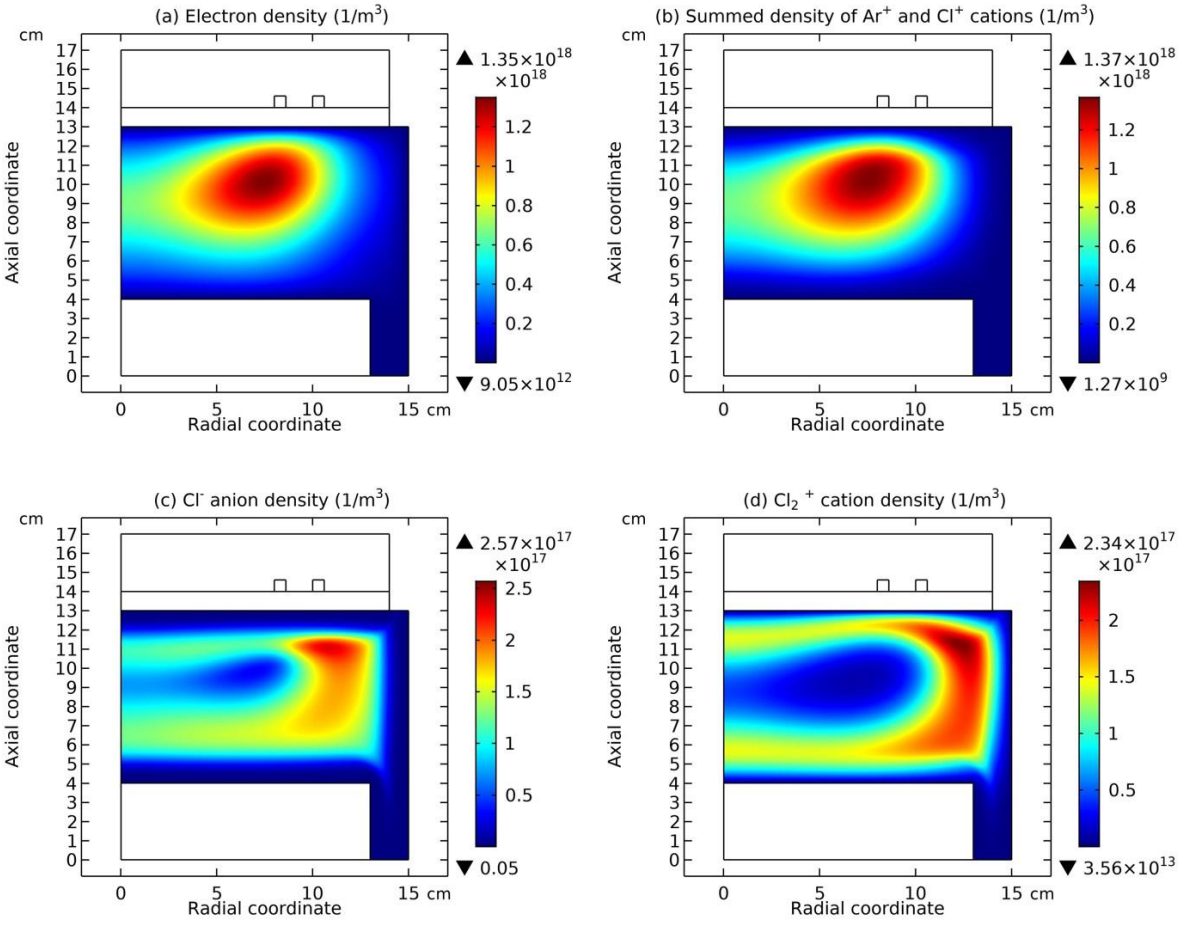

Figure 21: (a) Electron density, (b) summed Ar^+ and Cl^+ cations density, (c) Cl^- anion density, and (d) Cl_2^+ cation density of Ar/Cl_2 inductively coupled plasma at 5% Cl_2 content, 90mTorr and 300W, given by fluid simulation. Herein, the grouping effect is shown, where the coagulated electron and pair of Ar^+ and Cl^+ are grouped and individual hollow Cl^- and Cl_2^+ are grouped.

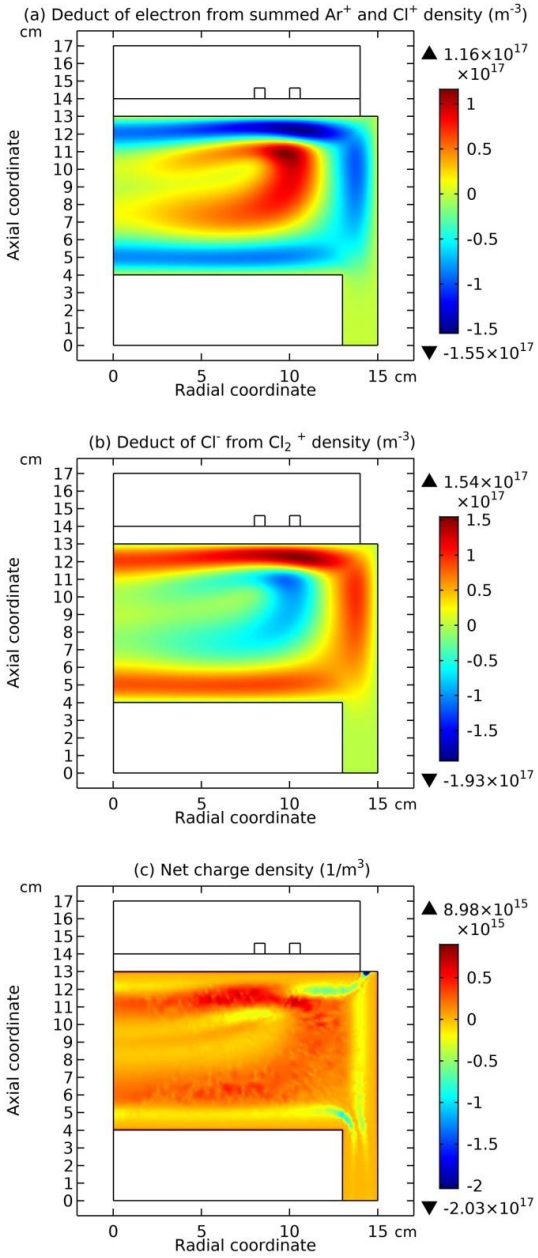

Figure 22: (a) Deduct of electron density from the Ar^+ and Cl^+ paired density, (b) deduct of Cl^- anion density from Cl_2^+ cation density, and (c) net charge density of Ar/Cl_2 inductively coupled plasma at 5% Cl_2 content, 90mTorr and 300W, given by fluid simulation. Herein, the grouping effect is shown more clearly, where the opposite charges of two same net charge profiles are given by the two groups, for basically satisfying the electric neutrality of plasma.

iii) Reactive feedstock gas depletion and shortage

Why the hollow anion density is happened when decreasing Cl_2 content? Because of the shortage of feedstock reactive gas, Cl_2 molecule. As shown in Fig. 23, at 5% Cl_2 and 90mTorr, as increasing the simulating time in fluid model simulation, the creation rate of Cl^- anion, i.e., attachments of electron with Cl_2, at first peaks under the coil and then sinks, finally exhibiting centric hollow shape, implying that the feedstock Cl_2 molecules have been severely depleted. In Fig. 24, the Cl_2 density at the different times of Fig. 23 are plotted. As seen, the feedstock is indeed consumed because of the small Cl_2 content in the feeding gas mixture.

In Fig. 25, the densities of neutrals, Cl_2, Cl and Ar, at 5% Cl_2 and 90mTorr are plotted. In Fig. 26, the axial profiles of these three densities under the dielectric window are given. It is seen that the Ar and Cl densities are high and the Cl_2 density is about two or three orders lower than the Ar and Cl at axially the discharge centre under the coil. This explains well the grouping effect, for Ar and Cl mainly generate Ar^+ and Cl^+, while Cl_2 gives rise to Cl_2^+ and Cl^-, from the point view of chemistry. That's why the electron (always at enough feedstock) and the pair of Ar^+ and Cl^+ cations are grouped, and Cl^- and Cl_2^+ are grouped. The latter is in the condition of feedstock gas shortage while the former is not.

It is noted that the gas inflow module is not considered in the present fluid simulation. However, the gas depletion still exists. When the gas inflow is included, the gas advection and gas heating probably influence the plasma transport. When the gas inflow is not included, the background gas is stagnant and cool. When the reactive gas concentration is very less, the strong dissociation reaction may severely deplete the feedstock molecules, i.e., the chorine molecules, Cl_2. So, the discussion of the discharge structure, hollow type, and the related self-grouping effect, are indeed significant. It is believed that the gas inflow and gas heating and the dissociation of electron-impact reaction are different processes, and the former is physics and the latter is chemistry.

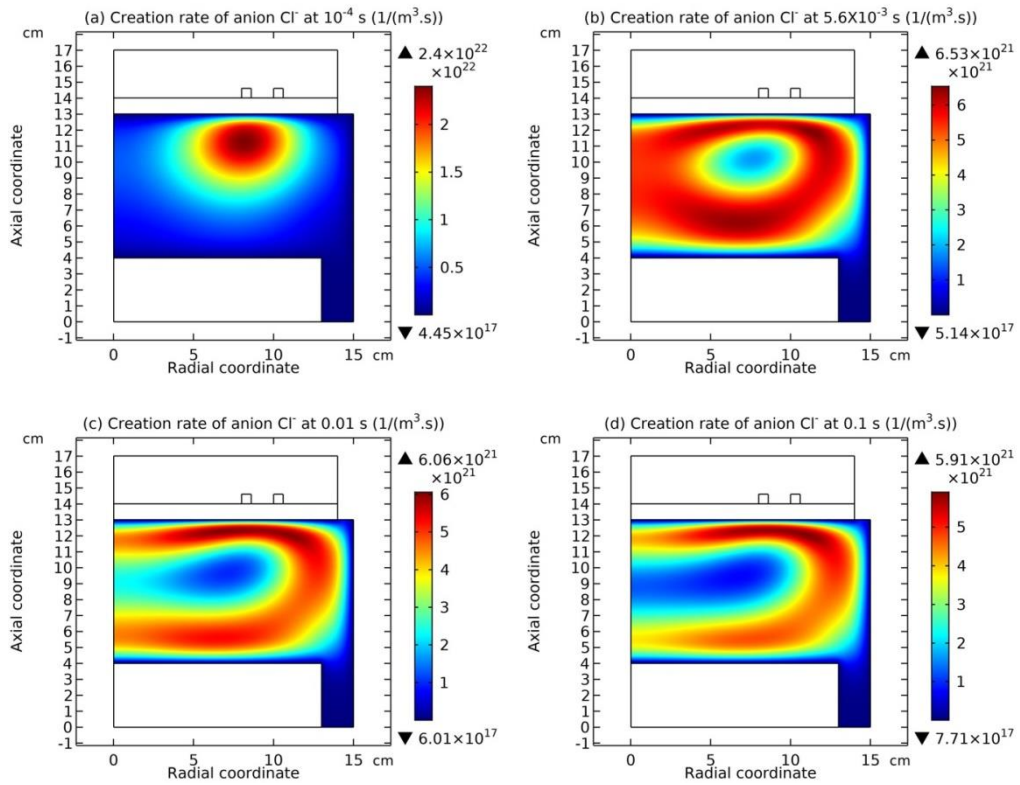

Figure 23: Creation rate of Cl^- anion at different times, (a) 10^{-4} s, (b) 5.6 x 10^{-3} s, (c) 0.01 s and (d) 0.1 s, in the Ar/Cl_2 inductively coupled plasma given by fluid simulation at 300W, 5% Cl_2 content and 90mTorr.

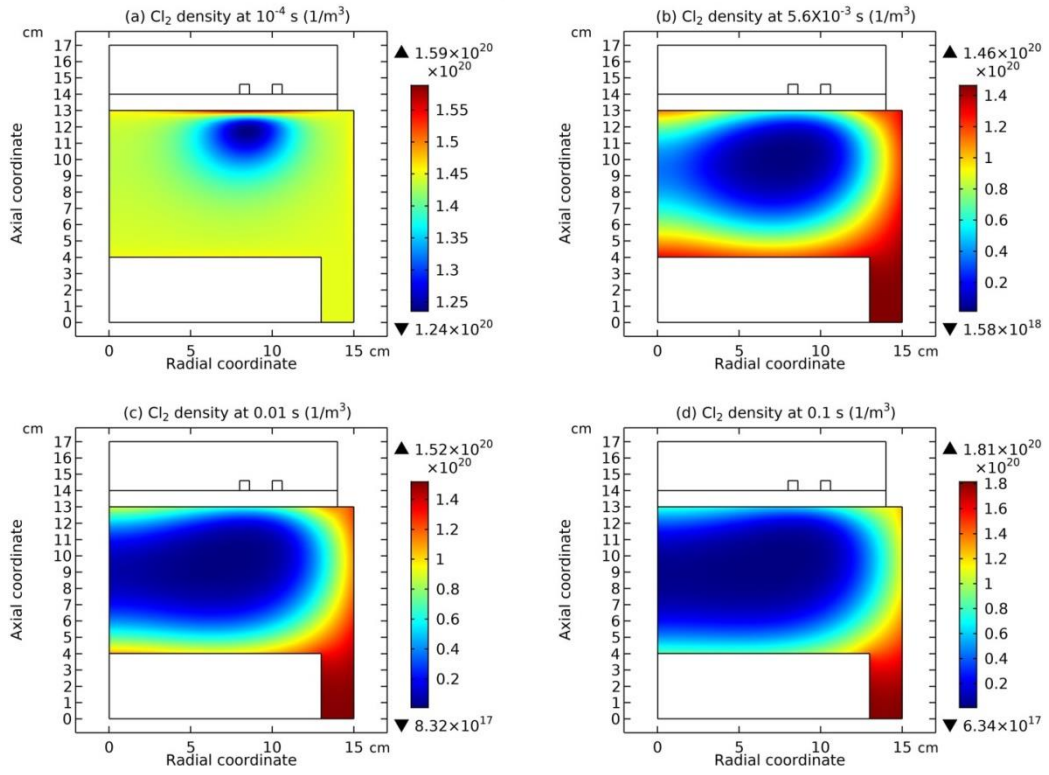

Figure 24: Density of one feedstock gas, Cl_2, of the Ar/Cl_2 inductively coupled plasma at different times, (a) 10^{-4} s, (b) 5.6 x 10^{-3} s, (c) 0.01 s and (d) 0.1 s, given by the fluid simulation at the discharge conditions of 300W, 5% Cl_2 content and 90mTorr.

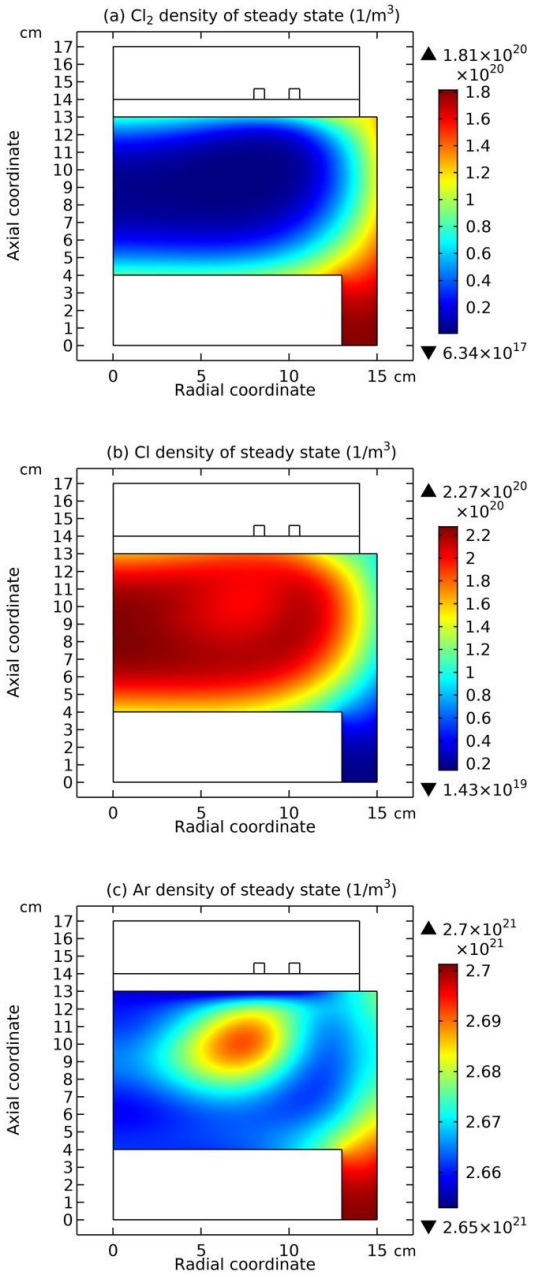

Figure 25: Densities of Cl_2 (a), Cl (b) and Ar (c) neutrals of steady state fluid model simulation in the Ar/Cl_2 inductive plasma at 300W, 5% Cl_2 content and 90mTorr.

iv) Electron coagulates at ambi-polar diffusion, without self-coagulation of species

In Fig. 27, the electron density and potential contour of 5% Cl_2 and 90mTorr Ar/Cl_2 plasma are given. As seen, when the self-coagulation-to-coil scheme is destroyed by the shortage of reactive feedstock, the electron coagulation shape is different. It does not attach the dielectric window anymore without the influence of ions self-coagulation.

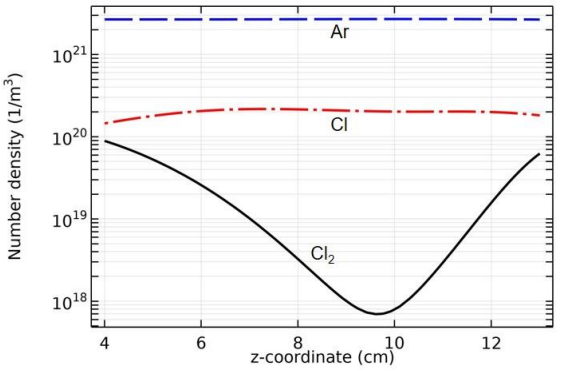

Figure 26: Axial profiles of Cl_2, Cl and Ar neutrals densities of steady state fluid simulation of Ar/Cl_2 inductively coupled plasma at 300W, 5% Cl_2 content and 90mTorr. The radial location is selected under the coil.

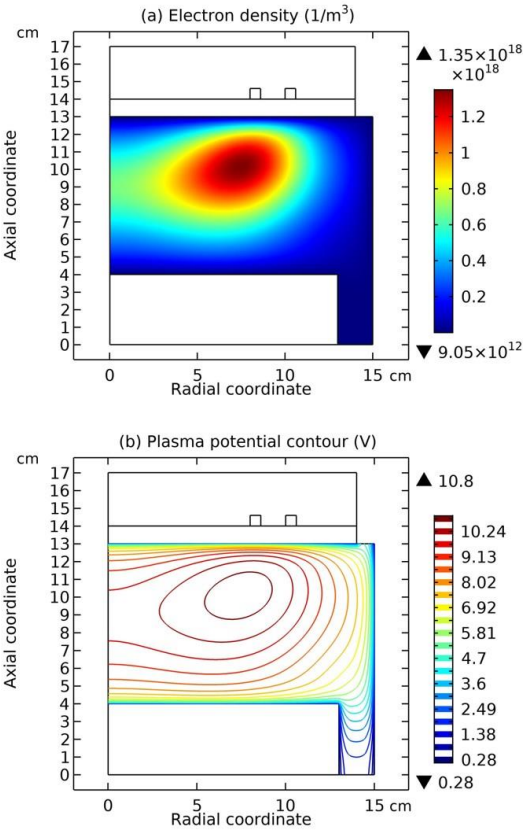

Figure 27: Electron density (a) and plasma potential (b) of Ar/Cl_2 inductively coupled plasma, given by fluid simulation at the discharge conditions of 300W, 5% Cl_2 content and 90mTorr.

This natural coagulation of electron is a general electropositive plasma feature at the high pressure. It originates from the fact that the electron ionization frequency of chemical term cannot be taken as constant in the electron continuity equation at the non-uniformity profile of electron temperature at high pressure. Hence,

the trigonometric or Bessel profile (i.e., the analytic solutions of continuity equation at constant frequency [5]) is not given, but forming the coagulated one. This is thus called the physical coagulation, relative to the chemical self-coagulation of ions (in electronegative core). Besides, the electron Boltzmann balance with plasma potential is automatically met as the peripheric self-coagulation of electron is neither happened herein (strong potential barrel at weak electronegativity).

III.d) Decreasing the pressure at low Cl_2 contents, e.g., 5%, from 90mTorr

i) From hollow to delta type and disappearance of grouping

In Fig. 28, when decreasing pressure at low Cl_2 content, 5%, the hollow anion density is disappeared and the delta type anion is reoccurred at 10mTorr. Furthermore, the grouping effect is disappeared as well. As shown in Fig. 29, at 10mTorr and 5% Cl_2, all cations densities hold the delta part as anion, at the advective ambi-polar self-coagulation.

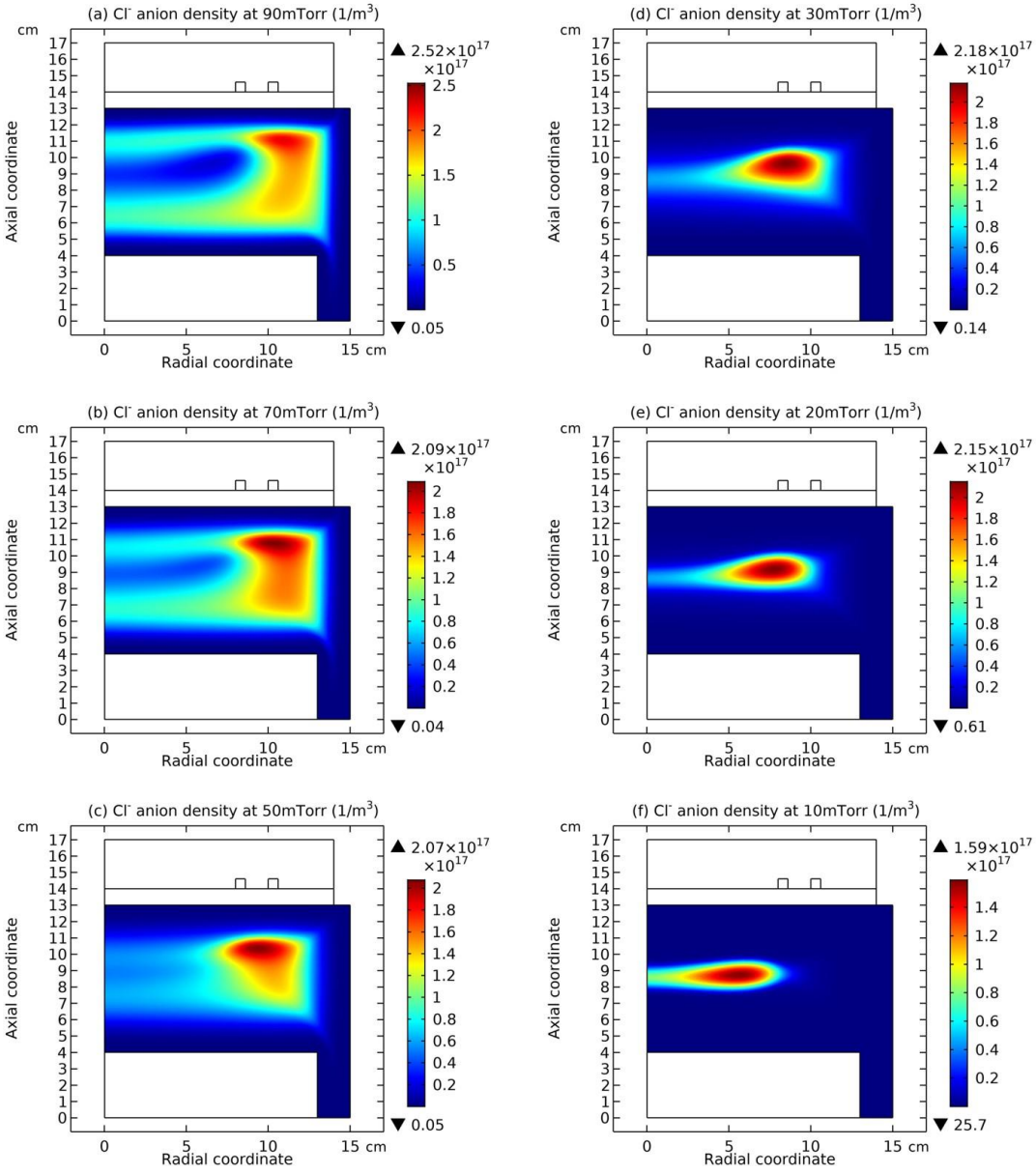

Figure 28: Cl^- anion density of Ar/Cl_2 inductively coupled plasma at different pressures, (a) 90mTorr, (b) 70mTor, (c) 50mTorr, (d) 30mTorr, (e) 20mTorr and (f) 10mTorr, given by the fluid model simulation at the discharge conditions of 300W and 5% Cl_2 content.

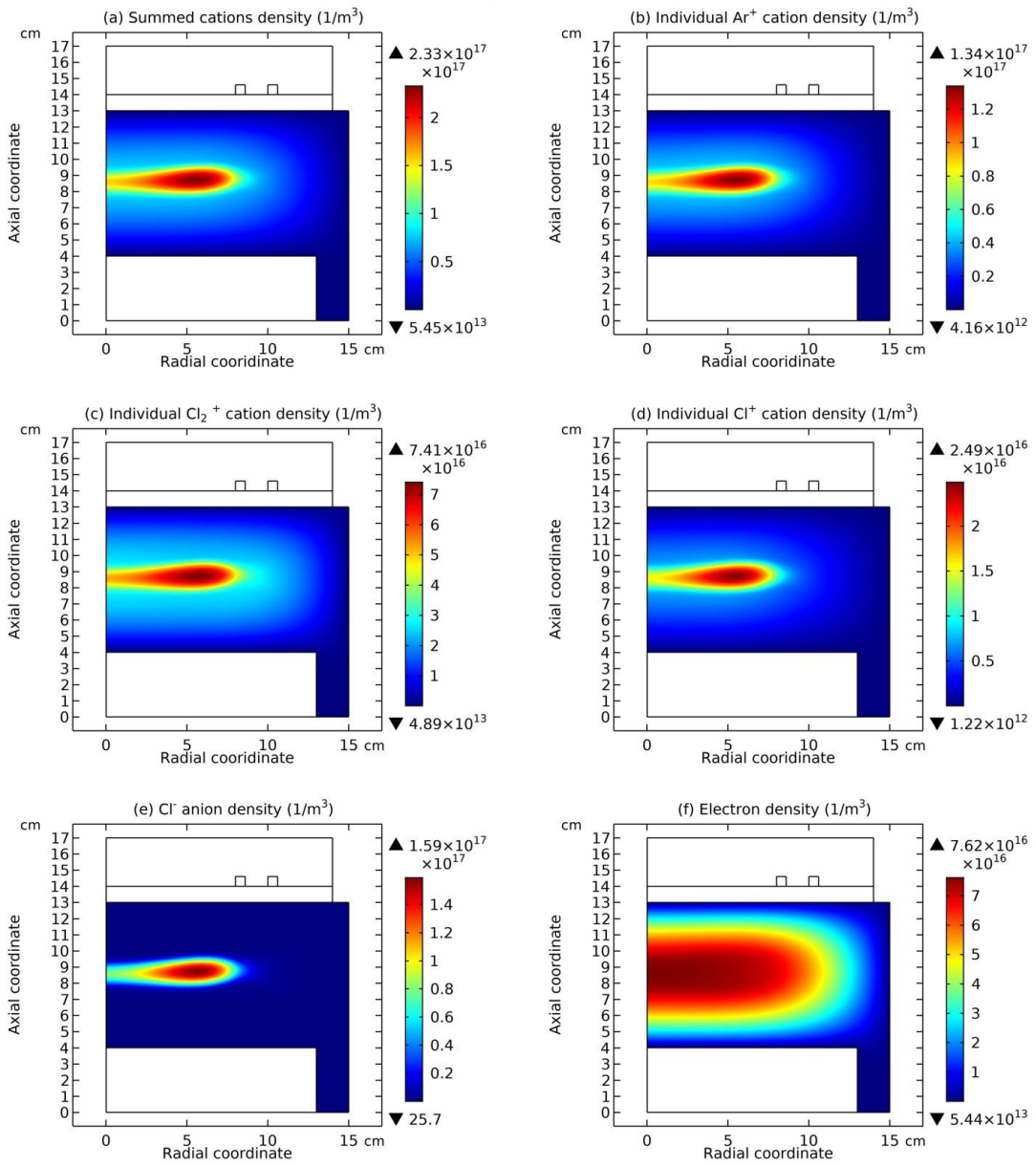

Figure 29: Summed cations density (a), the individual Ar^+ (b), Cl_2^+ (c) and Cl^+ (d) densities, Cl^- anion density (e) and the electron density (f) of Ar/Cl_2 inductively coupled plasma, given by the fluid model simulation at the discharge conditions of 300W, 5% Cl_2 content and 10mTorr.

ii) Refreshment of reactive feedstock gas and de-coagulation of electron

The disappearance of hollow anion and group effect is because electron density is low at low pressure in Fig. 30, which consumes less feedstock gases. So, the reactive feedstock gas is refreshed. Hence, the creation rate of anion is not centrically sunk at decreasing the pressure, as shown in Fig. 31.

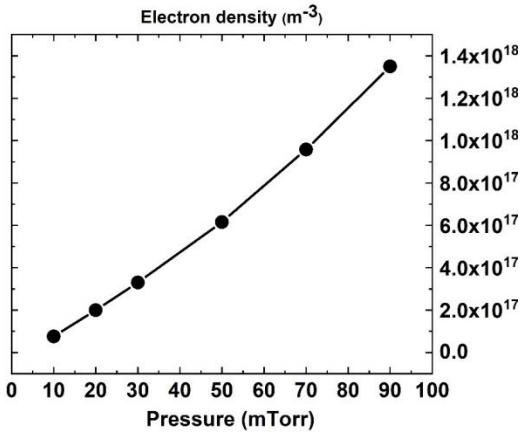

Figure 30: Electron density peak versus gas pressure, at 300W and 5% Cl_2 content, at fluid simulation.

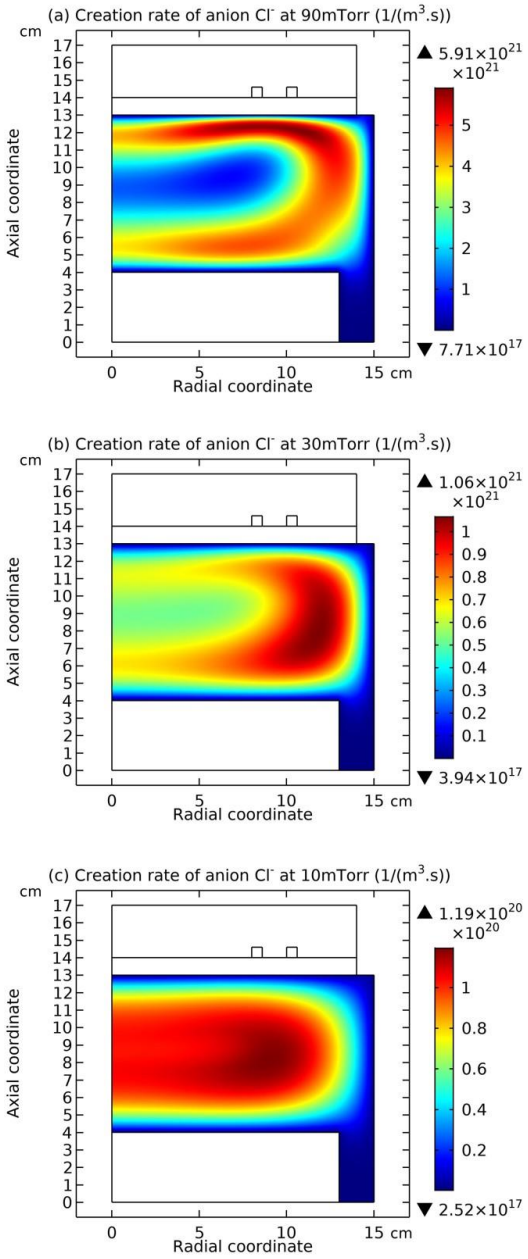

Figure 31: Creation rates of Cl^- anion at different pressures, (a) 90mTorr, (b) 30mTorr and (c) 10mTorr, of Ar/Cl_2 inductively coupled plasma given by the fluid model simulation at 300W, 5% Cl_2 content.

In Fig. 32, the Ar, Cl and Cl_2 densities axial profiles of 10mTorr and 5% Cl_2 are plotted. It is seen that the Cl_2 feedstock is just two times lower than the Ar and Cl, illustrating the group disappearance (for all charges species are now in enough feedstocks). In Fig. 33, it is shown that the electron coagulation is disappeared and it turns back to the trigonometric (along axis) and basic Bessel (along radius) profiles on decreasing the pressure at low Cl_2 content.

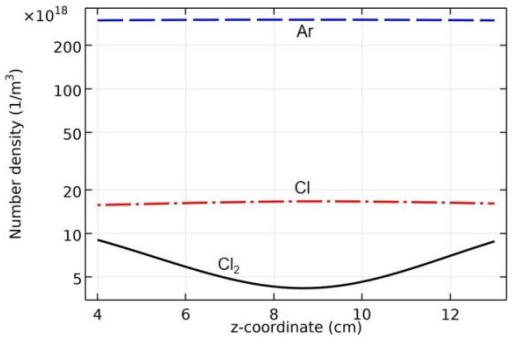

Figure 32: Axial profiles of Ar, Cl and Cl_2 neutrals densities of Ar/Cl_2 inductively coupled plasma given by the fluid model simulation at 300W, 5% Cl_2 content and 10mTorr, under the coil.

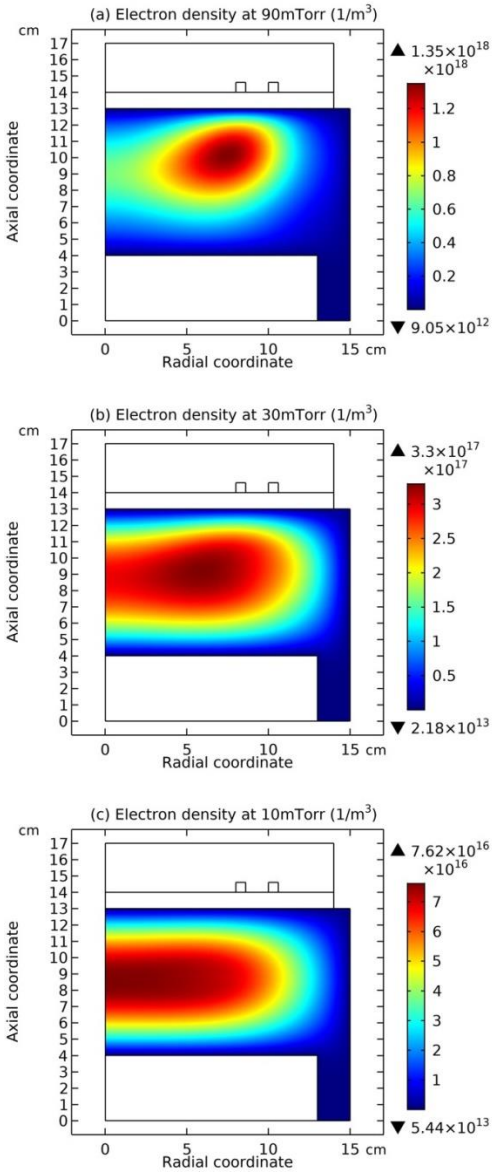

Figure 33: Electron density profile at different pressures, (a) 90mTorr, (b) 30mTorr and (c) 10mTorr, given by the fluid model simulation at 300W and 5% Cl_2 content. In this plot, the de-coagulation of electron is demonstrated.

This is logic, since at low pressure the transport (with larger diffusion coefficient and mobility than the high pressure) dominates over the chemical term, and the spatial variation of ionization frequency is negligible in the electron continuity equation. It is noted that due to the influence of delta anion, the radial profile of electron density herein is slightly deviated from the Bessel function, as illustrated in our previously reported Ar/O_2 inductively coupled plasma [17].

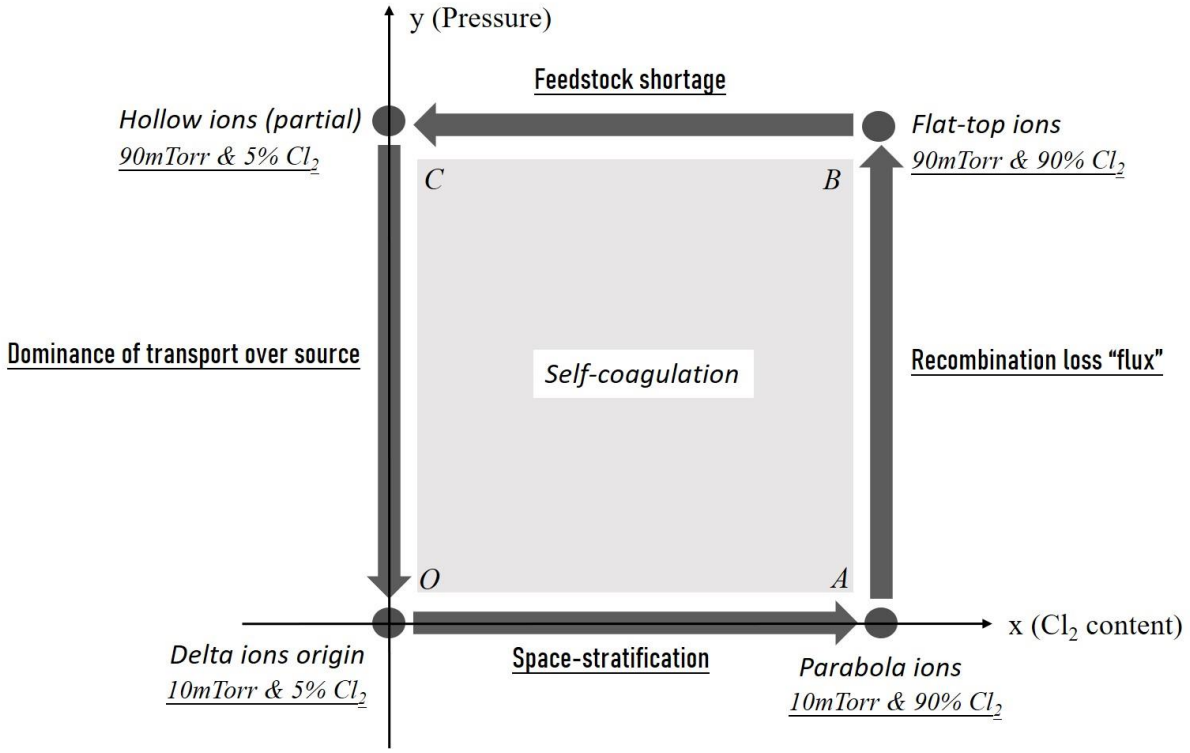

Figure 34: "Partial" overview of the cyclic study with respect to discharge conditions, i.e., pressure and reactive gas content concentration, at fixed power 300W and in the inductively coupled Ar/Cl_2 plasma given by fluid model simulation.

IV. Conclusion and further remarks

Partial contents of the cyclic study involving the pressure and Cl_2 content parameters of inductively coupled Ar/Cl_2 plasma at fixed power (300W) are schematically illustrated in a transformed Cartesian coordinate system, as shown in Fig. 34. The x axis represents the Cl_2 content, and y axis represents pressure, respectively. The origin of this system is about the delta anion, which is formed at 10mTorr and 5% Cl_2 content. Anion self-coagulation produces its own delta and cation delta is led to by the ambi-polar self-coagulation. So, the delta ions (here referring to both anion and cation) term is appeared at the origin. At the centre of drawn rectangle, the word, self-coagulation, is written, implying its importance and influence in almost all the processes occurring in the cycle. At increasing the Cl_2 content (along x axis) from the delta origin (O vertex of rectangle), after experiencing the space-stratification and core expansion, the parabola ions model is obtained, at 10mTorr and 90% Cl_2 content (vertex A). When increasing the pressure from the parabola ions, at the influence of so-called recombination loss flux [7], parabola turns into flat-topped model at 90mTorr and 90% Cl_2 content (vertex B). When decreasing the Cl_2 content at high pressure, the reactive feedstock gas shortage is met, and the partial hollow ions model is predicted, at 90mTorr and 5% Cl_2 content (vertex C). Eventually, when decreasing pressure (along y axis) back to 10mTorr at 5% Cl_2, the transport dominates over source term, and the delta ions model is re-obtained. This constructed rectangle describes the processes occurred in the cycle that are easily edited using this coordinate method (that's why a "partial" word is added in front of the overview in the caption of Fig. 34). It is stressed there are still many other important mechanisms, e.g., species-stratification (predicted by the analytics and repeated by simulation) hidden in the delta, concept of the gentle ambi-polar self-coagulation, drift essence of cation in the ambi-polar diffusion and self-coagulation, collapse of the self-

coagulation-to-coil scheme, discharge grouping effect, as well as the chemical (self-) and physical (ionization frequency is not constant) coagulations of electron and its de-coagulation. Besides, the diverse non-neutralities of plasma discovered at present are summarized, analysed, and classified, which helps people greatly understand the complex plasma. All these contents comprise this article.

Via the self-consistent fluid simulations, this article and its twin papers [16, 17] mainly about the Ar/O_2 and Ar/SF_6 inductively coupled plasmas, predicts so many new phenomena occurred in electronegative plasmas. From the tightly correlative analytic theories, all the new behaviours are well interpreted, reliable to readers. However, the validation of them through experiments is still needed, satisfying develop rules of scientific knowledges. This becomes our next work emphasis. Besides, the influences of other fluid model factors, such as the inertia term, the neutral gas heating and advection, and the more elaborate chemical reactions, on the above mechanisms are also very meaningful tasks for future.

V. Acknowledgement

This work is financially supported by the foundation of DUT19LK59, one fundamental research fund of central universities of China. Besides, the undergraduate student, Jinshuo Zhang, is thanked because of his study on revealing the transport essence of inductively coupled argon plasma via fluid model simulation (supervised by the author, Shu-Xia Zhao, as a teacher), when he was attending the National Undergraduate Plasma Scientific and Technological Innovation Contest of China. This study of him helped us understand the physical coagulation of electrons at high pressure and the de-coagulation of them at low pressure in the Ar/Cl_2 inductively plasma, at the very low Cl_2 content.

VI. References

[1] P. A. Miller, G. A. Hebner, K. E. Greenberg, P. D. Pochan, and B. P. Aragon, “An inductively coupled plasma source for the gaseous electronics conference RF reference cell,” *J. Res. Natl. Inst. Stand. Technol.*, Vol. 100, no. 4, 1995, pp. 427-439.

[2] S. Mouchtouris and G. Kokkoris, “A hybrid model for low pressure inductively coupled plasmas combining a fluid model for electrons with a plasma-potential-dependent energy distribution and a fluid-Monte Carlo model for ions,” *Plasma Sources Sci. Technol.*, vol. 25, no. 2, 2016, pp. 025007.

[3] F. Gao, S. X. Zhao, X. S. Li, and Y. N. Wang, “Comparison between experiment and simulation for argon inductively coupled plasma,” *Phys. Plasmas*, vol. 16, no. 2, 2009, pp. 113502.

[4] X. M. Han, X. L. Wei, H. J. Xu, W. Y. Zhang, Y. H. Li, et al, “Investigation on the parameter distribution of Ar/O_2 inductively coupled plasmas,” *Vacuum*, vol. 168, 2019, pp. 108821.

[5] M. A. Lieberman and A. J. Lichtenberg, Principles of Plasma Discharges and Materials Processing, 2nd ed. (Wiley-Interscience, New York, 2005).

[6] A. J. Lichtenberg, V. Vahedi, M. A. Lieberman and T. Rognlien, “Modelling electronegative plasma discharges,” *J. Appl. Phys.*, vol. 75, no. 5, 1994, pp. 2339-2347.

[7] A. J. Lichtenberg, I. G. Kouznetsov, Y. T. Lee, M. A. Lieberman, I. D. Kaganovich, et al, “Modelling plasma discharges at high electronegativity,” *Plasma Sources Sci. Technol.*, vol. 6, no. 3, 1997, pp. 437-449.

[8] P. Chabert and N. Braithwaite, Physics of Radio-Frequency Plasmas (New York: Cambridge University press, 2011) p.305.

[9] M. Lampe, W. M. Manheimer, R. F. Fernsler, S. P. Slinker and G. Joyce, “The physical and mathematical basis of stratification in electronegative plasmas,” *Plasma Sources Sci. Technol.*, vol. 13, no. 1, 2004, pp. 15-26.

[10] V. I. Kolobov and D. J. Economou, “Ion-ion plasmas and double layer formation in weakly collisional electronegative discharges,” *Appl. Phys. Lett.*, vol. 72, no. 6, 1998, pp. 656-658.

[11] I. G. Kouznetsov, A. J. Lichtenberg and M. A. Lieberman, “Modelling electronegative discharges at low pressure,” *Plasma Sources Sci. Technol.*, vol. 5, no. 4, 1996, pp. 662-667.

[12] I. G. Kouznetsov, A. J. Lichtenberg and M. A. Lieberman, “Internal sheaths in electronegative discharges,” *J. Appl. Phys.*, vol. 86, no. 8, 1999, pp. 4142-4153.

[13] S. V. Berezhnoj, C. B. Shin, U. Buddemeier, and I. Kaganovich, “Charged species profiles in

oxygen plasma," *Appl. Phys. Lett.*, vol. 77, no. 6, 2000, pp. 800-802.

[14] D. Vender, W. W. Stoffels, E. Stoffels, G. M. W. Kroesen and F. J. de Hoog, "Charged-species profiles in electronegative radio frequency plasma," *Phys. Rev. E*, vol. 51, no. 3, 1995, pp. 2436-2444.

[15] K. Kaga, T. Kimura, T. Imaeda and K. Ohe, "Spatial structure of electronegative Ar/CF_4 plasmas in capacitive RF discharges," *Jpn. J. Appl. Phys.*, vol. 40, no. 10, 2001, pp. 6115-6116.

[16] Y. Tian and S. X. Zhao, "Self-coagulation theory and related comet- and semi-circle-shaped structures in electronegative and gaseous discharging plasmas in the laboratory," *Appl. Sci.*, vol. 14, 2024, pp. 8041.

[17] S. X. Zhao, "Quasi-delta negative ions density of Ar/O_2 inductively coupled plasma at very low electronegativity," *Chin. Phys. B*, vol. 30, no. 5, 2021, pp. 055201.

[18] https://fr.lxcat.net/instructions/.

[19] E. G. Thorsteinsson and J. T. Gudmundsson, "A global (volume averaged) model of a chlorine discharge," *Plasma Sources Sci. Technol.*, vol. 19, no. 1, 2010, pp. 015001.

[20] S. Tinck, W. Boullart, and A. Bogaerts, "Simulation of an Ar/Cl_2 inductively coupled plasma: study of the effect of bias, power, and pressure and comparison with experiments," *J. Phys. D: Appl. Phys.*, vol. 41, no. 6, 2008, pp. 065207.

[21] M. V. Malyshev and V. M. Donnelly, "Diagnostics of inductively coupled chlorine plasmas: Measurement of Cl_2 and Cl number densities," *J. Appl. Phys.*, vol. 88, no. 11, 2000, pp. 6207-6215.

[22] D. Levko and L. L. Raja, "On the chemistry mechanism for low-pressure chlorine process plasmas," *J. Vac. Sci. Technol. B*, vol. 40, no. 5, 2022, pp. 052205.

[23] D. Levko, V. Subramaniam, and L. L. Raja, "Gas heating by inductively coupled low-pressure chlorine process plasmas," *Plasma Sources Sci. Technol.*, vol. 32, no. 12, 2023, pp. 125008.

[24] S. Y. Chung, Y. G. Yook, W. S. Chang, H. Choi, Y. H. Im, et al, "Spatially averaged global model of HBr/Cl_2 inductively coupled plasma discharges," *Phys. Plasmas*, vol. 31, no. 5, 2024, pp. 053502.

[25] A. Efremov, Y. Kim, H. W. Lee, and K. H. Kwon, "A comparative study of HBr-Ar and $HBr-Cl_2$ plasma chemistries for dry etch application," Plasma Chem. Plasma Process., vol. 31, no. 2, 2011, pp. 259-271.

[26] C. S. Corr, E. D. Pujo, P. Chabert, W. G. Graham, F. G. Marro, et al, "Comparison between fluid simulations and experiments in inductively coupled argon/chlorine plasmas," *J. Phys. D: Appl. Phys.*, vol. 41, no. 18, 2008, pp. 185202.

[27] V. I. Kolobov, "Striations in rare gas plasmas," *J. Phys. D: Appl. Phys.*, vol. 39, no. 24, 2006, pp. R487-R506.

[28] C. M. Ferreira, G. Gousset, and M. Touzeau, "Quasi-neutral theory of positive columns in electronegative gases," *J. Phys. D: Appl. Phys.*, vol. 21, no. 9, 1988, pp. 1403-1413.

[29] P. G. Daniels and R. N. Franklin, "The positive-column in electronegative gases – A boundary-layer approach," *J. Phys. D: Appl. Phys.*, vol. 22, no. 6, 1989, pp. 780-785.

[30] P. G. Danies, R. N. Franklin, and J. Snell, "The contracted positive-column in electronegative gases," *J. Phys. D: Appl. Phys.*, vol. 23, no. 7, 1990, pp. 823-831.

[31] R. N. Franklin, P. G. Daniels, and J. Snell, "Characteristics of electric-discharges in the halogens – the recombination-dominated positive-column," *J. Phys. D: Appl. Phys.*, vol. 26, no. 10, 1993, pp. 1638-1649.

[32] L. D. Tsendin, "Plasma stratification in a discharge in an electronegative gas," *Sov. Phys. Tech. Phys.*, vol. 34, no. 1, 1989, pp. 11-15.

[33] T. E. Sheridan, "Double layers in a modestly collisional electronegative discharge," *J. Phys. D: Appl. Phys.*, vol. 32, no. 15, 1999, pp. 1761-1767.

[34] T. E. Sheridan, P. Chabert, and R. W. Boswell, "Positive ion flux from a low-pressure electronegative discharge," *Plasma Sources Sci. Technol.*, vol. 8, no. 3, 1999, pp. 457-462.

[35] T. E. Sheridan, N. S. J. Braithwaite, and R. W. Boswell, "Relation between double layers and flux for a collisionless discharge with two negative components," 1999 *Phys. Plasmas*, vol. 6, no. 11, 1999, pp. 4375-4381.

[36] P. Chabert and T. E. Sheridan, "Kinetic model for a low-pressure discharge with negative ions," *J. Phys. D: Appl. Phys.*, vol. 33, no. 15, 2000 pp. 1854-1860.

VII. Appendix: The self-coagulation dynamics and theory

The continuity equation component of anions Cl^- that consists of free diffusion flux and negative source term (represented by the combination of Cl^- and Ar^+ ions) is expressed as

$$-D_{\mathrm{Cl}-}\nabla^2 n_{\mathrm{Cl}-} = -n_{\mathrm{Cl}-}n_{Ar+}k_{rec.} = -n_{\mathrm{Cl}-}\nu_{rec.}. \quad \text{(A1)}$$

Here, D_{Cl-} is the diffusion coefficient. k_{rec}, ν_{rec} are the rate constant and frequency of recombination. Making mathematic operations to Eq. (A1) and meanwhile omitting the subscript, Cl, for simplification, we get the Helmholtz equation as below.

$$\begin{aligned} &\nabla^2 n_{\mathrm{Cl}-} - n_{\mathrm{Cl}-}\frac{\nu_{rec.}}{D_{\mathrm{Cl}-}} = \nabla^2 n_{\mathrm{Cl}-} - n_{\mathrm{Cl}-}k^2 = 0, \\ &\nabla^2 n - nk^2 = 0. \end{aligned} \quad \text{(A2)}$$

Reform the Helmholtz equation with the method of separation of variables in the cylindrical coordinate system, at the assumption of azimuthal symmetry.

$$\begin{aligned} &\frac{1}{\rho}\frac{\partial}{\partial\rho}\left(\rho\frac{\partial n}{\partial\rho}\right) + \frac{\partial^2 n}{\partial z^2} - k^2 n = 0, \\ &n(\rho, z) = R(\rho)Z(z), \\ &Z'' + \nu^2 Z = 0, \\ &\frac{d^2R}{d\rho^2} + \frac{1}{\rho}\frac{dR}{d\rho} - \left(k^2 + \nu^2\right)R = 0. \end{aligned} \quad \text{(A3)}$$

Here, ν^2 represents the eigenvalues.

With the homogeneous boundary conditions of axial ordinary differential equation, $Z''+ \nu^2 Z=0$, the discrete eigenvalues of ν^2 are acquired, so are the eigen functions, $Z_m(z)$.

$$\begin{aligned} &{\nu_m}^2 = m^2\pi^2 / l^2, \\ &Z_m = \sin(m\pi z / l), \\ &\mathrm{Z} = \sum_{m=0}^{\infty} c_m Z_m = \sum_{m=0}^{\infty} c_m \sin(m\pi z / l). \end{aligned} \quad \text{(A4)}$$

As noted, the radial ordinary differential equation, $\frac{d^2R}{d\rho^2} + \frac{1}{\rho}\frac{dR}{d\rho} - \left(k^2 + {\nu_m}^2\right)R = 0,$ is one zero-order imaginary Bessel equation, because of the property of negative source. Considering that the density value is limit at the axial centre, the imaginary Bessel function, not the Hankel function, is applied. So, we get the expression of R(r) as follow,

$$R = d_m I_0(\sqrt{k^2 + {\nu_m}^2}\rho) = d_m I_0(\sqrt{k^2 + m^2\pi^2 / l^2}\rho). \quad \text{(A5)}$$

Finally, we obtain the expression of n(ρ,z) as,

$$\begin{aligned} n(\rho, z) = R(\rho)Z(z) &= \sum_{m=0}^{\infty} c_m \sin(m\pi z / l)\cdot d_m I_0(\sqrt{k^2 + {\nu_m}^2}\rho) \\ &= \sum_{m=0}^{\infty} a_m \sin(m\pi z / l)\cdot I_0(\sqrt{k^2 + m^2\pi^2 / l^2}\rho). \end{aligned} \quad \text{(A6)}$$

Next, special mathematic skills are applied to Eq. (A6), and a delta distribution that is independent on the spatial coordinates are deduced, which represents the self-coagulation dynamics and explains the delta-comet type of anions profile. More details about the self-coagulation theory can be found in Ref. [17].

$$
\begin{aligned}
n(\rho,z) &= R(\rho)Z(z) = \sum_{m=0}^{\infty} a_m \sin(m\pi z/l)\cdot I_0(\sqrt{k^2+m^2\pi^2/l^2}\,\rho) \\
&= \lim_{m\to\infty}\left[a_m \sin(m\pi z/l)\cdot\infty\right] = \lim_{m\to\infty}\left[a_m \sin(m\pi z/l)\cdot\lim_{z\to 0}\frac{1}{z}\right] \\
&= \lim_{z\to 0}\left[\lim_{m\to\infty} a_m \sin(m\pi z/l)\cdot\frac{1}{z}\right] = \lim_{z\to 0}\left[\lim_{m\to\infty} a_m \cdot\frac{\sin(m\pi z/l)}{z\pi/l}\cdot\frac{\pi}{l}\right] \\
&= \lim_{\zeta\to 0}\left[\lim_{m\to\infty} a_m^{'}\cdot\frac{1}{\pi}\frac{\sin(m\zeta)}{\zeta}\right] = \lim_{\zeta\to 0}\left[a_\infty^{'}\lim_{m\to\infty}\frac{1}{\pi}\frac{\sin(m\zeta)}{\zeta}\right] \\
&= a_\infty^{'}\lim_{\zeta\to 0}\delta(\zeta).
\end{aligned}
\tag{A7}
$$